Supplementary Materials for

In vivo modeling of human neuron dynamics and Down syndrome

Raquel Real[1,2#], Manuel Peter[3#], Antonio Trabalza[1#], Shabana Khan[1], Mark A. Smith[1], Samuel J. Barnes[4], Ayiba Momoh[3], Alessio Strano[3], Joana Dopp[1], Emanuela Volpi[5], Graham Knott[6], Frederick J. Livesey[3,7*] and Vincenzo De Paola[1*]

*Corresponding author. Email: vincenzo.depaola@imperial.ac.uk; r.livesey@ucl.ac.uk

[#]These authors contributed equally to this work.

This PDF file includes:

Other Supplementary Materials for this manuscript includes the following:

Materials and Methods

Generation of iPSC cultures

Human stem cell research was approved by the Steering Committee for the UK Stem Cell Bank and for the Use of Stem Cell Lines. Skin biopsies were collected from donor individuals with Down Syndrome by the University of Cambridge Dept. of Psychiatry, following approval of the Cambridgeshire Research Ethics Committee, with informed consent from the donor or representative. Samples were designated anonymous identifiers following collection. Skin punch biopsies were subdivided and cultured at 37°C in 5% CO2 in DMEM + Glutamax (Thermo Fisher Scientific) supplemented with 10% foetal calf serum, penicillin (50 U ml−1), and streptomycin (50 µg ml−1) and 1 mM Sodium Pyruvate (Sigma) until fibroblast outgrowth was observed. When plates were confluent, fibroblasts were trypsinized and transferred to T75 dishes for further expansion. Cellular reprogramming of fibroblasts was carried out using Cytotune 2.0 Sendai Reprogramming kits (Thermo Fisher Scientific) according to the manufacturers protocol, and established using feeder free conditions in Essential-8 media (Thermo Fisher Scientific). Cells were grown in Essential-8 medium (Thermo Fisher Scientific) as feeder free cultures on Geltrex (Thermo Fisher Scientific) coated plates and maintained at 5% CO2 at 37°C in a humidified incubator.

Primary skin fibroblasts from a Ts21 donor were reprogrammed using non-integrative Sendai viruses and obtained clones showed high expression levels of the stem cell pluripotency factor Oct4 (Fig. S1C). Clones were genotyped for the presence of the extra copy of human chromosome 21 (Hsa21) using a Taq Man copy number assay with probes for APP and Down Syndrome Critical Region 1 (DSCR1), two genes located on Hsa21. All clones showed the presence of three copies of APP and DSCR1 indicating trisomism of Hsa21 (Fig. S1A). During this initial screen we also found one clone from the trisomic donor that was disomic for APP and DSCR1 indicating a loss of the extra copy of Hsa21 during the re-programming process. Throughout this study we further used published disomic control (WT-1, NDC1.2, non-demented control) (*53*) and trisomic human iPSCs (Ts21-1) (*54*) (Fig. S1A) and compared those to our trisomic/revertant disomic pair.

Directed differentiation of human iPSCs

Directed differentiation of iPSCs to cortical excitatory neurons was carried out as previously described (*8*). Briefly, 24 h before the start of differentiation iPSCs were passaged with 0.5 mM EDTA and plated at high density. Upon reaching 100% confluence the neuronal induction was started (Day 0). The medium was changed to neuronal maintenance medium supplemented with 10 µM SB431542 (Tocris) and 1 µM Dorsomorphin (Tocris) and was changed daily. On day 12 the neuroepithelial sheet was lifted off with Dispase (Thermo Fisher Scientific), broken up to small clumps and plated on laminin (Sigma) coated plates in neuronal maintenance medium supplemented with 10 µM SB431542 and 1 µM Dorsomorphin. On the next day (Day 13), the media was changed to neuronal maintenance medium supplemented with 20 ng ml^{-1} Fibroblast growth factor 2 (FGF2; PeproTech). Medium was changed every other day and FGF2 was removed from the medium on day 17. Cells were split with Dispase at a 1:2 ratio when neuronal rosettes started to meet. On day 25 cells were dissociated with Accutase (Thermo Fisher Scientific) and plated at a 1:1 ratio on laminin coated plates. Cell were

expanded 1:2 when they reached 90% confluence until day 33. On day 31-33 they were infected with high titer lentiviruses. Neurons were engrafted between day 36 and 38.

Neuronal maintenance medium (1 L) consisted of 500 ml DMEM:F12 + glutamax (Thermo Fisher Scientific), 0.25 ml Insulin (10 mg ml^{-1}, Sigma), 1 ml 2-mercaptoethanol (50mM Thermo Fisher Scientific), 5 ml non-essential amino acids (100 X Thermo Fischer Scientific), 5 ml Sodium Pyruvate (100 mM, Sigma), 2.5 ml Pens/Strep (10000 U/µl, ThermoFisher Scientific), 5 ml N2 (ThermoFisher Scientific), 10 ml B27 (Thermo Fisher Scientific), 5 ml Glutamax (100 X, Thermo Fisher Scientific) and 500 ml Neurobasal (Thermo Fisher Scientific) medium.

Copy number assay *in vitro*

Neurons were grown in neuronal maintenance medium, harvested with Accutase and genomic DNA was isolated with the DNeasy Blood & Tissue kit (Quiagen) following the manufacturers protocol. The presence of an extra copy of chromosome 21 was determined using a TaqMan copy number assay (Thermo Fisher Scientific) for APP (Hs01180853_cn, Thermo Fisher Scientific) and DSCR1 (Hs01114326_cn, Thermo Fisher Scientific) according to the manufacturers protocol using 5 µl genomic DNA.

Gene expression analysis *in vitro*

RNA was collected from day 35-36 cultures and profiled with a custom Nanostring gene expression panel of approximately 250 genes. After subtracting the maximum negative control probe counts, gene counts were normalized using the geometric mean of 6 positive control probes and of 7 housekeeping genes (CLTC, GAPDH, GUSB, PPIA, RPLP1, RPS15A, RPS9).

Western blot *in vitro*

Whole cell protein extraction was performed by lysis of cell pellets in RIPA buffer supplemented with protease inhibitors tablets (Roche) and phosphatase inhibitors (Thermo Scientific) before removal of the soluble fraction. Western blot analysis was carried out using the following antibodies: β-actin, anti-APP C-Terminal Fragment, Tuj1, Synapsin1 and PSD95.

Cell line identity verification

Genomic DNA was extracted from iPSC clones using DNeasy Blood & Tissue kit (Qiagen) following the manufacturers protocol and profiled with PowerPlex 16 HS Multiplex STR assay (Promega). Genotype of third allele in trisomy lines was extrapolated from electropherogram peak height.

Genome-wide copy number SNP assay

Genomic DNA was extracted from iPSC clones using DNeasy Blood & Tissue kit (Qiagen) following the manufacturers protocol and sent for SNP analysis using the Infinium HumanCytoSNP-12 platform (Illumina), except for the WT-1 sample, which was run on CytoSNP850K platform (higher density). Data was processed using GenomeStudio 2.0 and CNV-region-report-v2.1 (Illumina).

Lentiviral production

Third generation lentivirus was produced by calcium phosphate transfection of HeK293T cells with pBOB-Syn-GFP or pBOB-Syn-GCaMP6s-P2A-tdTomato plasmids and complemented with the packaging plasmids pRSV-Rev and pMDLg/pRRE and the VSVG envelope plasmid pMD2.G.

Animals

Adult immunodeficient mice (*n* = 57; 3-4 month-old; NOD-SCID gamma, Charles River, UK) were used for all *in vivo* imaging experiments. All mice were given access to food and water *ad libitum* and maintained in a 12-hour light-dark cycle. All procedures were conducted by researchers holding a UK personal license and conducted in accordance with the UK Animals (Scientific Procedures) Act 1986.

Craniotomy and human neuron transplantation

Cranial windows were surgically implanted over the somatosensory cortex as previously described (*30*). Mice were anaesthetized with ketamine-xylazine intraperitoneal injection (0.083 mg/g ketamine, 0.0078 mg/g xylazine) and then administered intramuscular dexamethasone (0.02 ml at 4 mg/ml), to reduce inflammation, and subcutaneous bupivacaine (1 mg/kg), a local anesthetic. A few drops of lidocaine (1 % solution) were applied on the skull surface prior to a ~5 mm diameter craniotomy being drilled over the somatosensory cortex. Neurons previously transduced (DIV 31) with a lentiviral vector (LV) carrying either a GFP or a calcium reporter gene under the neuron-specific Human Synapsyn-1 promoter (LV-hSyn-GFP and LV-hSyn-GCaMP6s-2A-tdTomato, respectively) were dissociated with 1 ml accutase enzyme mix (Sigma), centrifuged and washed at 1200 rpm in PBS, before being resuspended in 15-20 microliters of cortex buffer for cell counts.

We injected 20,000 cells in two sites spaced 0.5 mm apart (i.e. 40,000 cells in total in 1 μl) in the AP axis at coordinates: AP -1.8; L +2.8; V -0.5 mm from bregma (i.e. the somatosensory cortex barrel field) using a micro pump (UMP-3, World Precision Instruments, USA) and a microelectrode (< 50 μm at the tip).

A glass coverslip was then placed over the craniotomy and sealed with cyanoacrilic veterinary glue and dental cement. The exposed skull was subsequently covered in dental cement and a metal bar included on the top for positioning at the two-photon microscope stage. Mice were allowed to recover for 21 days before imaging.

Two-Photon imaging *in vivo*

A purpose built two-photon microscope (Prairie Technologies) equipped with a tunable coherent Ti:Sapphire laser (Coherent) and PrairieView acquisition software was used for all imaging experiments. Mice were anaesthetized with oxygen and isoflurane mix (0.6-1.5 %) and secured to the microscope stage with the head metal bar attached to a custom-built fixed support. Eye ointment (Lacri-lube) was applied to the eyes to prevent dehydration and the temperature was maintained at around 36 °C by a heating pad. An Olympus 4 X objective with a 0.13 numerical aperture (NA) was used to identify characteristic blood vessels to reliably relocate regions-of-interest (ROIs) at each imaging time point. Olympus 20 X (NA = 1.2), 40 X (NA = 0.8) and 60 X (NA = 0.9) water immersion objectives were then used to acquire several ROIs per animal (GFP: 75 x 75

μm field of view, 512 x 512 pixels for neurite imaging and 50 x 50 μm field of view, 1024 x 1024 pixels for synaptic imaging, 1 μm step size; GCaMP6-tdTomato: 300 x 300 μm field of view, 256 x 256 pixels, single plane). A pulsed 910 nm laser beam was used with typical power never exceeding 70 mW on the back focal plane.

For calcium imaging, mice were lightly anaesthetized and transduced cells were identified using the TdTomato signal at 1040 nm. Four minutes recording sessions were then acquired at 3 Hz with the 920 nm laser to excite GCaMP6s. GCaMP6-expressing neurons have been shown to display normal physiological properties including input resistance, resting membrane potential, input–output relationship, synaptic input maps, and normal synaptic plasticity (*55*). Moreover, we found no difference between GFP and GCaMP6s expressing human neurons in terms of their biophysical/synaptic properties (unpaired *t*-test, $P > 0.05$).

Electron microscopy

Immediately after the last imaging session, the mouse was perfused with a buffered solution of 2.5% glutaraldehyde and 2% paraformaldehyde. The brain was then removed and serial 60-micron thick sections cut tangentially to its surface at the region of the previous live imaging. The sections were then stained with heavy metals and embedded in resin. Blocks were made in the region of the graft area which was visible in the resin embedded sections. Thin sections were cut at 50 nm thickness and collected on single slot grids. These were further stained and imaged in a transmission electron microscope (Tecnai, FEI Company).

Correlated 2-photon-serial electron microscopy

We reconstructed 41 dendritic spines, which had been imaged previously *in vivo* on a Ts21-1 neuron. Immediately after the last imaging session, the mouse was perfused with a buffered solution of 2.5% glutaraldehyde and 2% paraformaldehyde. The brain was then removed and serial 60-micron thick sections cut tangentially to its surface at the region of the previous live imaging. These sections were then imaged again in the 2-photon microscope and laser marks burnt around the exact dendrites of interest. The sections were then stained with heavy metals and embedded in resin. Blocks were made around the visible laser marks and imaged using block face scanning microscopy (Gatan 3View and Zeiss Merlin scanning electron microscope). Serial images were taken of the regions of interest, and these were aligned using the FIJI software, and the dendrites and axonal boutons reconstructed using the TrakEM2 tools. The 3D structure of the reconstructed dendrite and presynaptic boutons (**Fig. 4F**) was created with Blender software (version 2.57; Blender Foundation, http://www.blender.org).

Electrophysiology

Coronal slices (350 μm) containing the somatosensory cortex (Bregma -0.3 to +1.4 mm) were maintained at room temperature (22-25ºC) in an external solution containing (in mM) NaCl 125, KCl 2.5, NaH_2PO_4 1.25, $NaHCO_3$ 25, $CaCl_2$ 2, $MgCl_2$ 1, D-glucose 10, D-mannitol 15, equilibrated with 95% O_2, 5% CO_2, pH 7.4. Human neurons were visualized in the somatosensory cortex by the expression and excitation of GFP. Whole-cell current-clamp (I_{fast}) and voltage-clamp recordings were made at ~35 °C using borosilicate glass pipettes (4-8 MΩ) containing (in mM) Kgluconate 130, KCl 10, EGTA

0.5, NaCl 1, $CaCl_2$ 0.28, $MgCl_2$ 3, Na_2ATP 3, GTP 0.3, phosphocreatine 14 and HEPES 10 (pH 7.2). Neurons were also voltage-clamped at -70 mV using a modified internal solution in which Kgluconate was replaced with CsCl (130 mM). Slices were bathed in (+)-bicuculline (20 µM) for miniature excitatory currents (mEPSC) or NBQX for miniature inhibitory currents (mIPSC). For anatomical inspection, Lucifer-yellow-CH (1 mg/ml) was added to the internal electrode solution. Following access to the whole-cell configuration, Lucifer-yellow was allowed to dialyze the neuron for 10-15 minutes before gradually withdrawing the patch electrode from the cell. Slices were fixed in 4% (w/v) paraformaldehyde and permeabilized in PBS containing 0.4% (v/v) Triton-x and 2% (v/v) chicken serum. Slices were incubated with a rabbit anti-Lucifer-yellow antibody for 2-3 days at 4 °C and then incubated with a chicken anti-rabbit antibody conjugated with Alexa-594. Slices were mounted on glass coverslips prior to 2-photon imaging. Synaptic kinetic analysis was performed only on cells with at least 40 recorded events.

Immunohistochemistry, histology and related analysis

Neurons *in vitro* were washed with PBS and fixed with 4% PFA for 10 minutes, then blocked in a 5% normal goat serum in TBS + 0.3% Triton X-100 solution, incubated overnight with primary antibodies (**Supplementary Table 1**), and with the appropriate Alexa-dye conjugated secondary antibodies (1:500, Thermo Fisher Scientific) diluted in TBS + 0.3% Triton X-100. 4',6-Diamidino-2-Phenylindole (DAPI, 5 µg/ml final concentration) was used for nuclear counterstaining. Imaging was performed on an inverted Leica TCS SP8 scanning confocal microscope (Leica Microsystems). 4 µm image stacks were acquired and the z projection was used for counting cells using a custom automated ImageJ (NIH) script.

At the end of the live imaging experiments, animals were anesthetized with an overdose of ketamine and xylazine, and then perfused intracardially with PBS followed by 4% paraformaldehyde (PFA). Brains were fixed overnight in 4% PFA. Coronal brain sections were cut at 40 µm in a vibratome (Leica VT1000S) and stored free-floating in PBS with 0.01% NaN_3. For the cellular characterization of the grafts, consecutive sections containing the graft were blocked in a 10% donkey serum with 0.5% Triton X-100 PBS solution, and then incubated overnight with primary antibodies (**Supplementary Table 1**). Sections were then incubated with appropriate secondary antibodies (1:1000, Alexa Fluor®, Thermo Fisher Scientific). All incubations were performed in 5% donkey serum with 0.1% Triton X-100 PBS solution. When using primary antibodies raised in mouse and rat in the same tissue sections, primary and secondary antibody incubations were performed sequentially to avoid the anti-rat secondary antibody cross-reacting with mouse immunoglobulins. Sections were mounted using ProLong® Gold Antifade Mountant (Thermo Fisher Scientific). All sections stained with anti-NuMA antibody required a sodium citrate (10 mM, pH 6) heat-mediated antigen retrieval procedure. Brain sections were imaged with either a scanning confocal TCS SP5 II or SP8 microscope (Leica Microsystems), using a 20 X (NA 0.75) or oil-immersion 40 X objective (NA 1.45). ROIs were randomly selected within the graft area. A customised semi-automated script was used to analyze images with nuclear markers in FIJI. Briefly, nuclei were segmented and intensity values of segmented objects measured across all channels after background subtraction. Threshold levels were set to define positive objects. The criteria for threshold selection was elimination of type I error while

minimising the occurrence of type II error (<10%). Astrocytes (GFAP+) and oligodendrocyte progenitors (PDGFRα+) were manually counted in FIJI. Microglia was analysed using a custom Cell Profiler pipeline (Bloomfield et al, *in press*).

For the volumetric assessment of the graft, ROIs were drawn around human-specific Neural Cell Adhesion Molecule (hNCAM)-labelled human graft and each of their areas measured from every second consecutive coronal mouse section (total 48 sections, 140 μm apart) in ImageJ. Volume was calculated from the sum of areas, section thickness, and interval, according to Cavalieri's principle (*56*), and independently confirmed with *Imaris* image analysis software (Bitplane).

Teratoma formation was excluded and vascularization confirmed (20 out of 20 grafts) by inspection of H&E stained material by an expert pathologist.

For mapping axonal projections at 5 mpt, sections at 120 μm intervals were selected across the entire brain (n = 3), and immunostained for hNCAM (Supplementary Table 1) as above. All sections were imaged with an epifluorescence microscope (Olympus IX70) using a 20 X objective (NA 0.5, 0.321 μm pixel size). The Allen Mouse Brain Atlas (Paxinos and Franklin, 2001) was used to identify brain areas of interest. Image analysis was performed by manual counting of fibers using ImageJ. A color scheme with a range from grey (no projections) to bright red (more than 100 projections) was used to indicate the relative amount of axonal projections in each brain area.

Retrograde trans-synaptic tracing

TVA expressing lentivirus was produced as described previously using the pBOB-SYN-HTB plasmid (Addgene plasmid # 30195). Neurons were infected with the lentivirus expressing rabies glycoprotein (G), TVA and nuclear GFP (LV-hSyn-G-TVA-NLS-GFP) at day 30. The medium was changed the next day to remove the virus and neurons were stereotactically injected into the somatosensory cortex of adult NSG mice, as previously described. After 5 months, an EnvA-pseudotyped, G-deleted mCherry expressing rabies virus (EnvA + RV*dG*-mCherry) was injected in the same location. Animals were perfused 7 days later with 4% PFA intracardially, and the brains fixed overnight in 4% PFA. Coronal brain sections were cut at 50 μm in a vibratome, and stained with anti-human nuclei (hNu), anti-GFP and anti-DsRed antibodies (Supplementary Table 1), as described above. All regions of interest containing mCherry positive cells throughout the whole brain were imaged with a confocal Leica SP5 microscope using a 20 X objective (NA 0.7), and quantifications of mCherry+/hNu+ and mCherry+/hNu- input cells were performed by manual counting using ImageJ.

Fluorescence In Situ Hybridization (FISH) and analysis

Brain sections (40 μm) were dehydrated in ethanol series (30%, 50% and 70%). Sections were allowed to air dry at room temperature for 1 day, re-hydrated in PBS and then permeabilised in PBS with 0.5% Triton X-100. A heat-mediated step with sodium citrate buffer (10 mM, pH 6) was performed. Slides were transferred to 2x SSC, and afterwards equilibrated in a 2x SSC with 50% formamide solution for at least 4 hours, at room temperature. After applying the Hsa21 probe (XL 21q22/XCP 21, Metasystems), a coverslip was sealed with rubber cement and then slides were allowed to rest for 1h at room temperature, to allow probe penetration in the section. Slides were incubated at 80 °C for 5 minutes and then at 37 °C in a dark humidified chamber for 2 days, to allow

hybridization to occur. Slides were washed in 2x SSC at 37 °C, and then counterstained with DAPI (1:1000, Thermo Fisher Scientific). Sections were mounted using ProLong® Gold Antifade Mountant (Thermo Fisher Scientific) and imaged with a Leica SP5 confocal laser scanning microscope using an oil-immersion 63 X (NA 1.45) objective, z-stack range of 5-18 planes.

Analysis was carried out manually in 3D. Cell nuclei within Z-stacks obtained by confocal microscopy were individually evaluated and annotated blind to genotype using ImageJ (NIH). Nuclei that appeared to be either truncated or damaged, or overlapped with other nuclei, or showed significant background 'noise' were not included in the scoring. A minimum of 50 nuclei from a minimum of two different Z-stacks were evaluated for each line. Based on the observed number of fluorescent hybridization signals, nuclei were assigned to four different categories, namely 'one signal', 'two signals' 'three signals' and '> three signals'. Data gathered by FISH analysis on histological sections of grafts originating from euploid lines indicated that the assay met the sensitivity and specificity parameters generally recommended for FISH testing, >95% and >98% respectively (358 nuclei analyzed in total). On histological sections of grafts originating from Down syndrome cell lines, the presence of an extra copy of chromosome 21 was confirmed by evaluating the frequency of the triple fluorescent pattern ('three signals' nuclei/total nuclei) and by comparing it to the specific cut-off threshold values calculated from the normal reference ranges (*CRITBINOM,* 95% Confidence Level).

Data Analysis

Neurite length quantification. Image stacks from *in vivo* two-photon images were processed with Image J (section alignment, background subtraction, brightness and contrast adjustment). Neurites were then manually traced from a clear reference point in the maximum intensity projections for length measurement.

Dendritic spine/bouton dynamics. Quantifications were made at 3-4 mpt. Dendritic spine/bouton density was determined by blindly annotating dendritic spines/boutons in Matlab using custom made software (*57*) and metrics calculated in the following way:

• Total number of boutons/spines reported in the text and figure legends were calculated as the total number in the first session plus the number of gains across all imaging sessions (i.e. each synaptic structure was counted only once).

• Density of boutons/spines at any given time point a was defined as Density(a) = $n_a/length_a$.

• Turnover rate (TOR) was defined as (nG + nL)/(2*N), where nG and nL are the numbers of bouton/spine gains and losses respectively, and N is the total number of boutons/spines present in the same time interval. These total numbers include repeated counts of the same boutons/spines, in case they were present in more than one session.

• Gains and losses fractions between session a and b were defined as Gains(a; b) = $nG_{(b-a)}/N_{(a+b)}$ and Losses(a; b) = $nL_{(b-a)}/N_{(a+b)}$. N includes repeated counts of the same boutons/spines, in case they were present in more than one session.

• Survival fraction (Fr) was defined by the cumulative sum of EPBs/spines that survive at each time point (t), divided by the total number of EPBs/spines that were present at session 1:

$$Fr(T) = \left[\sum_{t=1}^{T} n_t\right]/n_1$$

***In vivo* calcium imaging**. Time-series were pre-processed in ImageJ using the moco plugin for registration (*58*), followed by the application of a 3D median filter (2 x 2 x 2, in x-y-z, respectively).

Analysis of sparse calcium activity. Neurons were selected based on the mean normalized maximum intensity projection of the data by hand and the nucleus was excluded from selection. Fluorescence traces were calculated as the average fluorescence of pixels lying within the cell in each frame. To remove slow changes in raw fluorescence traces, the 15th percentile value of the fluorescence distribution was subtracted from the raw fluorescence signal. $\%\Delta F/F_0$ signals were calculated by dividing the raw fluorescence signal by the median of each cells fluorescence distribution and normalizing to the background calcium signal. Cellular activity was calculated using the integrated fluorescence as describe previously (*59*) with a 15% $\Delta F/F_0$ threshold. Activity was then normalized to the duration of our imaging paradigm to give values in $\%\Delta F/F_0$/second, as described previously (*60*).

Burst activity analysis. We defined bursts as global events where > 95% of the peak pixel intensity was above the threshold defined above, across each imaged cortical area. All regions were then visually inspected to further validate the presence of global events.

Global activity analysis. Global analysis was the same as that for sparse activity, but for this analysis activity was measured over the entire region of interest.

Burst direction. For each event we calculated the peak of the first derivative of the $\%\Delta F/F_0$ transient at 8 spatial positions (based on breaking the image into a 3 x 3 grid and excluding the central square) in the imaged cortical region. We then took the time of the peak derivative value at each of the 8 spatial positions during a calcium event. Polar plots were calculated by taking the difference of each time-point from the earliest time-point, thus generating lag values for each of the 8 spatial positions. We then averaged lag values over all the events in the imaged region (10 – 40 events). We calculated the direction selectivity index (DSI) for each region as follows: $1 - R_{null}/R_{best}$, where R_{best} is the interpolated response to the direction with the longest lag and R_{null} is the interpolated response to the position opposite the direction with the longest lag. Regions of interest with a DSI value > 0.3 where considered to have a burst direction. Directionality of calcium bursts was not due to scanning artefacts as it did not always follow scanning direction.

Whisker stimulation responses. Following visual inspection of average $\% \Delta F/F_0$ calcium data, we found that 1 out of 3 animals exhibited time-locked responses to whisker stimulation. To examine whether these responses were indeed sensory driven or attributable to the contaminating effects of burst activity we developed a simple metric. A trial was considered to be driven by sensory stimulation if it had no response in a ten second baseline period, and a clear transient time locked to the onset of the whisker stimulation. To test how often our metric gave a false positive, we used randomly selected epochs of spontaneous activity that were matched in duration to our sensory stimulation trials as a control.

Statistical analyses were performed in GraphPad Prism V7 and SigmaPlot V13. All measurements are given as the mean ± standard error of the mean (SEM), unless otherwise stated. Results were considered significant when $P < 0.05$. The normality test used was the

Shapiro-Wilk test. Figures were prepared using Adobe Photoshop and Illustrator. Images in figures 1G, 1H, 1I, 1I', 1J, 2B (bottom panel), 2G, 2H, 4A, 4E, 4J and S20 are best projections in x-y-z of neuronal, dendritic or axonal stacks. Movies S4-6 were processed with mean 3D filtering and shown at the indicated frame per second (fps).

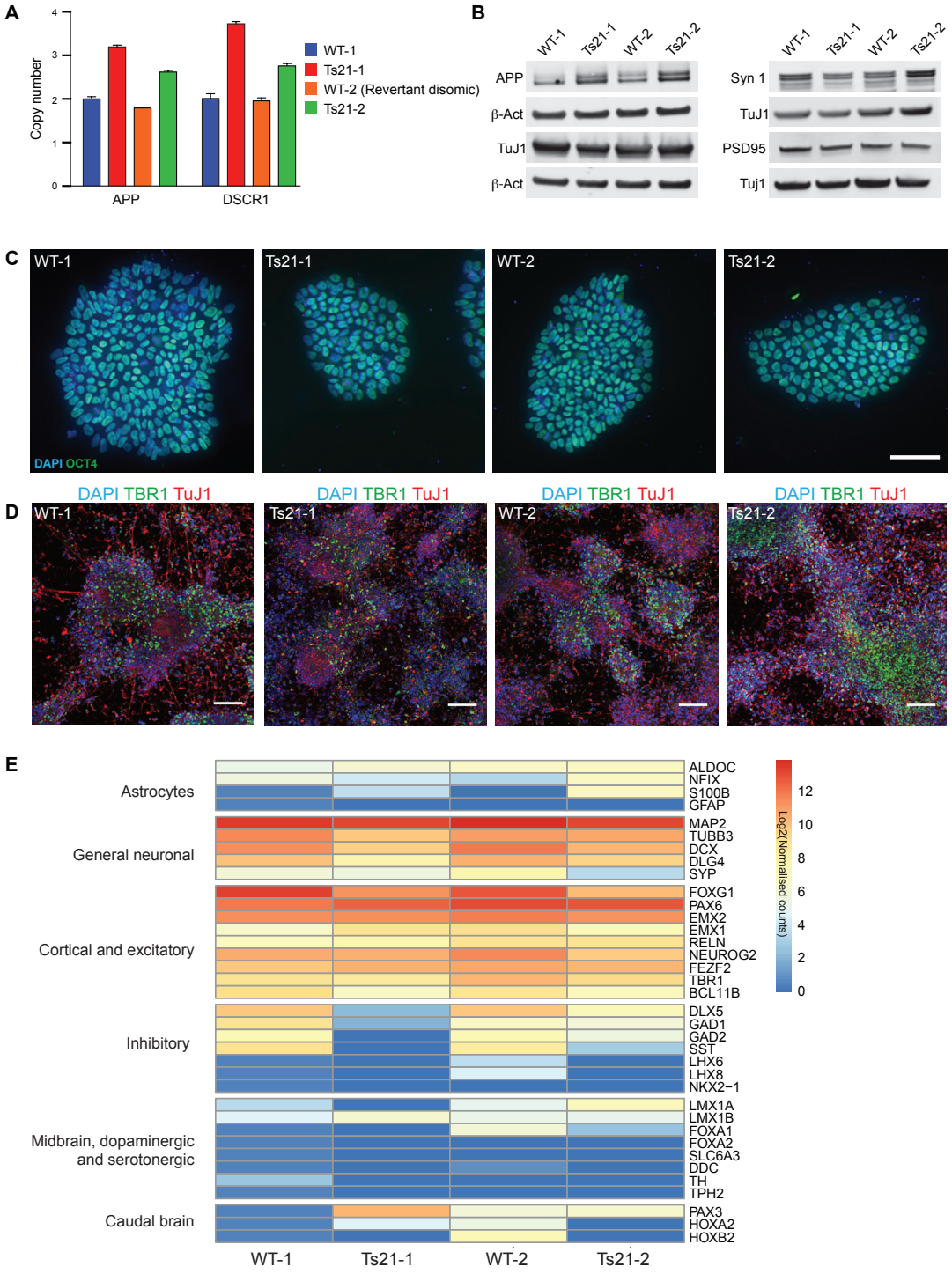

Figure S1. Characterization of human iPSC lines. (**A**) TaqMan copy number assay for APP and DSCR1in control and Ts21 neurons. Trisomic neurons have an extra copy of APP and DSCR1. WT-2 is a revertant disomic cell line from Ts21-2. (**B**) Western blot detection of APP, Tuj1, Syn1 and PSD95 at day 58. Ts21 neurons show normal levels of Tuj1, Syn1 and PSD95 but increased levels of APP compared to control neurons. (**C**) Re-programmed human iPSCs express the stem cell self-renewal factor OCT4. Scale bar, 50

μm. (**D**) Confocal image stacks of Ts21 and control neurons at day 50 immunostained for the neuronal marker Tuj1 and the deep layer marker TBR1. Scale bars, 100 μm. (**E**) Gene expression analysis of day 35-36 cultures. Heatmap of log2 normalised counts for selected genes expressed in the indicated brain regions and/or cell types. Note selective cortical identity. Each column of the heatmap is one sample run once.

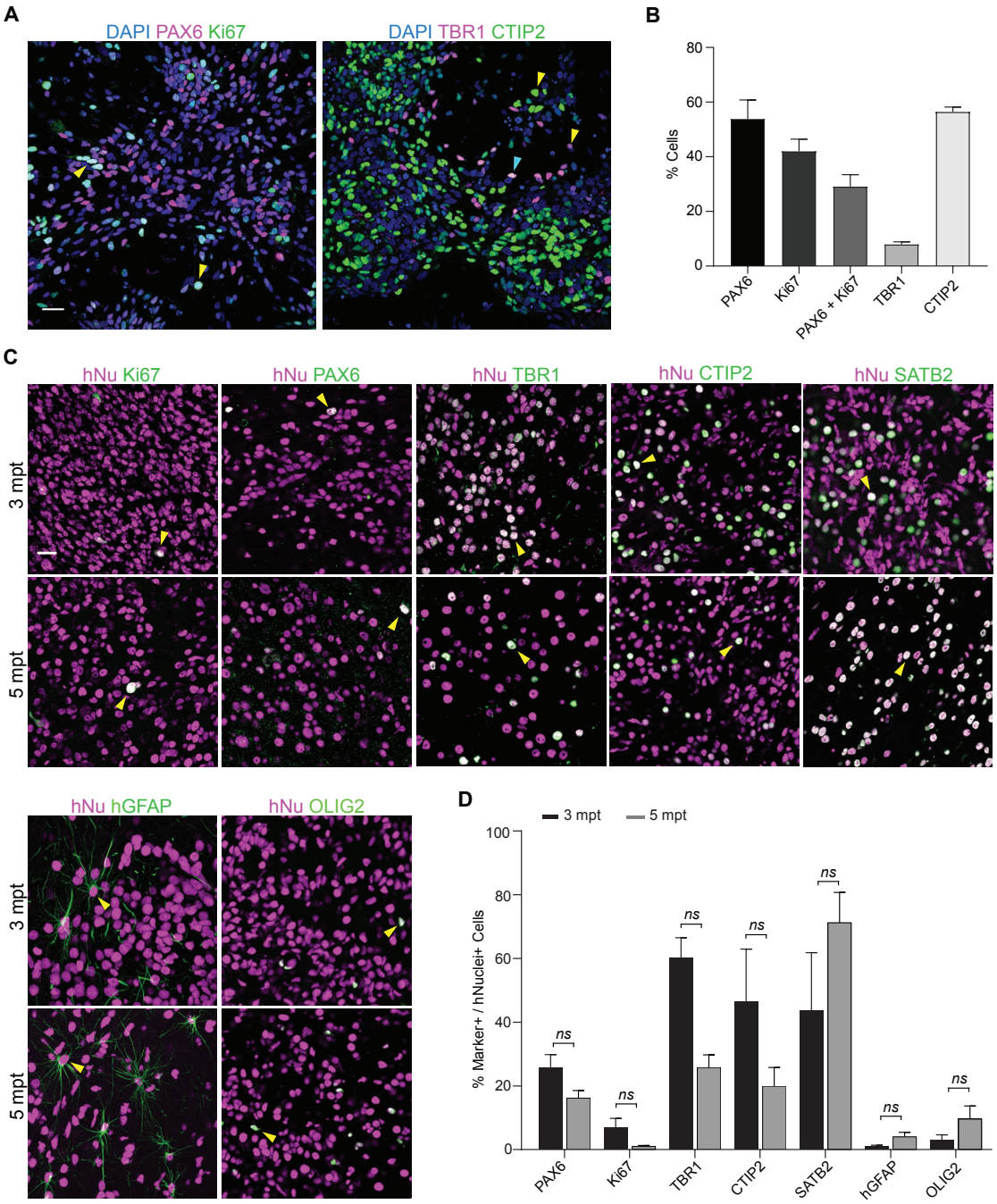

Figure S2. Maturation of diverse cell types in human tissue grafts. (**A**) Representative immunostaining at 36 days post-differentiation of human iPSC-derived neurons for DAPI, PAX6 (neuronal progenitor marker), Ki67 (proliferation marker), TBR1and CTIP2 (deep cortical layer markers). Yellow arrowheads indicate examples of proliferating neural progenitor cells (PAX6+/Ki67+, left) and neurons with deep layer identity (either CTIP2+ or TBR1+, right) and light blue indicates an example of a CTIP2+/TBR1+ nucleus. Scale bar, 30 µm. (**B**) Quantification of cell populations *in vitro* at day 36 post-differentiation (*n* = 4 wells). (**C**) Representative immunostaining of human grafts 3 and 5 months after transplantation for hNu (human nuclei marker), Ki67, PAX6, TBR1, CTIP2, SATB2

(upper cortical layer marker), Glial Fibrillary Acidic Protein (hGFAP, human astrocytic marker) and Oligodendrocyte Transcription Factor 2 (OLIG2, oligodendrocyte marker); arrowheads indicate examples of positive human cells. Scale bar, 20 μm.
(**D**) Quantification of cell populations *in vivo* at 3 and 5 mpt ($n = 3$ animals for each time point; hNu+ nuclei sampled per cell marker: 2994 ± 487 and 3283 ± 245 at 3 and 5 mpt respectively, mean ± SD). Sidak's multiple comparison test after one-way ANOVA; *ns*, not significant. Data are represented as mean ± SEM.

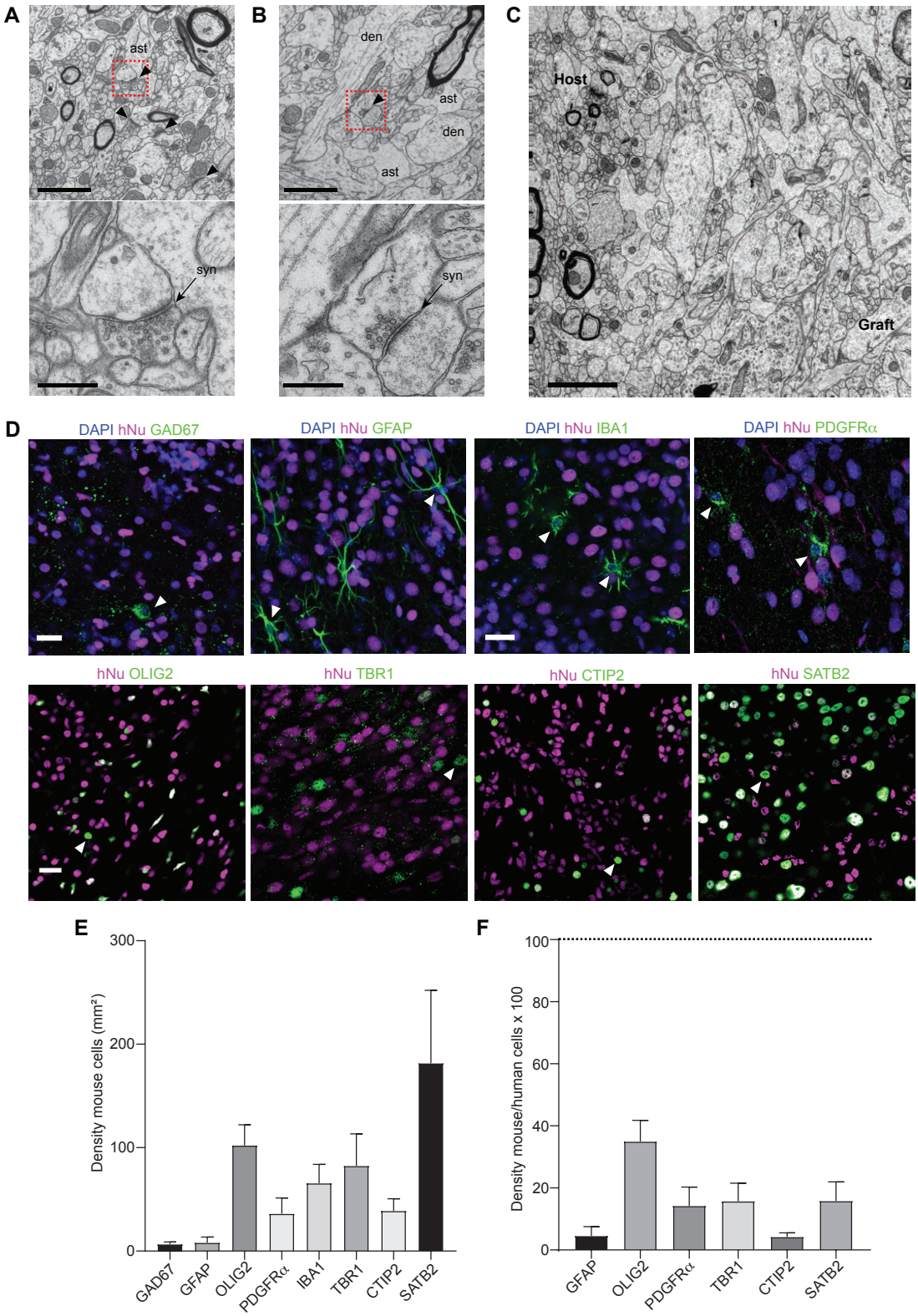

Figure S3. Graft ultrastructure and host-derived cell identity. (**A**) Representative electron microscopy image of neuropil of mouse cortex immediately adjacent to the graft.

A number of synapses (arrowheads) are present. The bottom panel is a magnified image of the region highlighted by the red box. Scale bars, 2 μm (top) and 0.5 μm (bottom). (**B**) Representative electron microscopy image of the human graft. Fewer synapses are present (enlarged example in bottom panel). ast, astrocytic profiles. den, dendrite. syn, synapse. Scale bars, 2 μm (top) and 0.5 μm (bottom) (**C**) Representative electron microscopy image of the interface between the human graft and the host brain tissue. Scale bar, 3 μm. (**D**) Representative immunostaining of human grafts 5 mpt for glutamic acid decarboxylase 67 (GAD67, inhibitory interneuron marker), platelet-derived growth factor receptor α (PDGFRα, oligodendrocyte precursor marker), ionized calcium-binding adapter molecule 1 (Iba1, microglia marker), GFAP, OLIG2, TBR1, CTIP2 and SATB2. Arrowheads indicate examples of positive mouse cells. Scale bar, 20 μm. (**E**) Quantification of mouse cell density in the graft (n = 3 mice; area sampled per cell marker: 1.54 ± 0.03 mm^2, mean ± SD). (**F**) Mouse cell density in the graft normalized to the respective human cell density (dashed line; n = 3 mice; area sampled per cell marker: 0.80 ± 0.08 mm^2, mean ± SD).

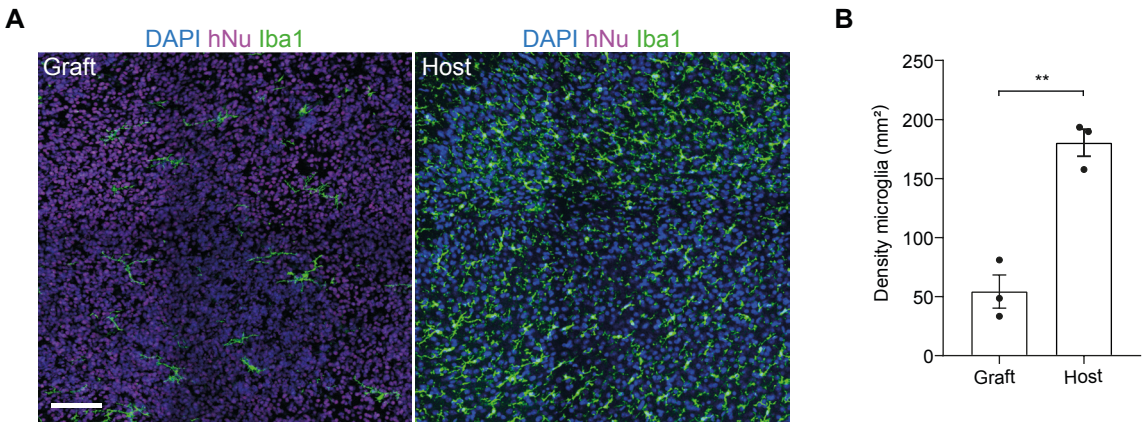

Figure S4. Minimal recruitment of mouse-derived microglia in the human tissue graft. (**A**) Representative example of Iba1/hNu staining at 3 mpt. Scale bar, 100 µm. (**B**) Quantification of microglia density at 3 mpt (n = 3 mice) in the graft (area sampled: 5.2 ± 1.5 mm^2, mean ± SD) and respective contralateral host cortex (area sampled: 2.4 ± 0 mm^2, mean ± SD). Paired t-test, $^{**}P < 0.01$. Each data point represents an animal.

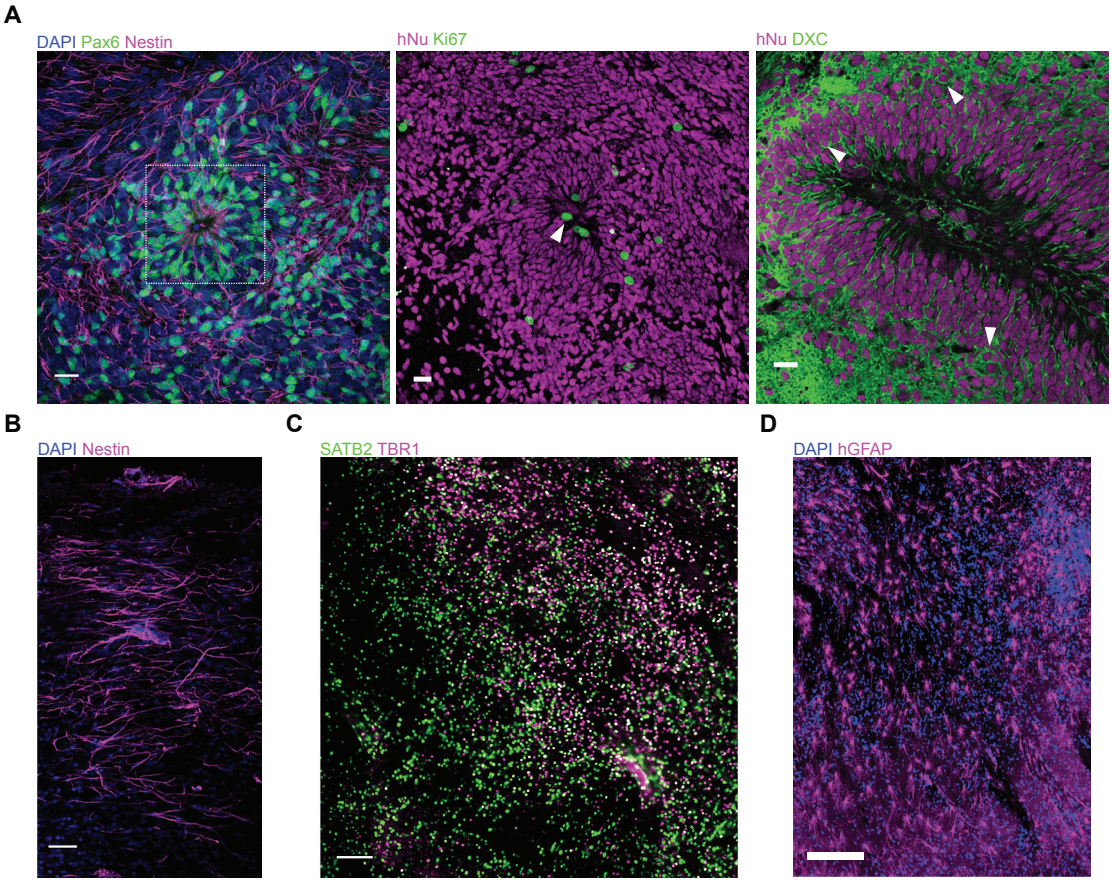

Figure S5. Complex cytoarchitecture in human cortical tissue grafts.
(**A**) Representative immunostaining of neural rosette-like structures in the human tissue grafts 2 mpt for PAX6, Nestin (radial glia marker), Ki67 and doublecortin (immature neuronal marker, DXC); arrowheads indicate examples of positive human cells. The highlighted region in the first image depicts the core of the neural rosette at its centre. Scale bars, 20 µm. (**B**) Representative immunostaining of Nestin-positive processes at 2 mpt. Scale bar, 50 µm. (**C**) Representative immunostaining of the human grafts at 5 mpt for TBR1 and SATB2. Scale bar, 100 µm. (**D**) Representative immunostaining of the human graft for hGFAP at 5 mpt. Note the homogeneous distribution of human astrocytes. Scale bar, 200 µm.

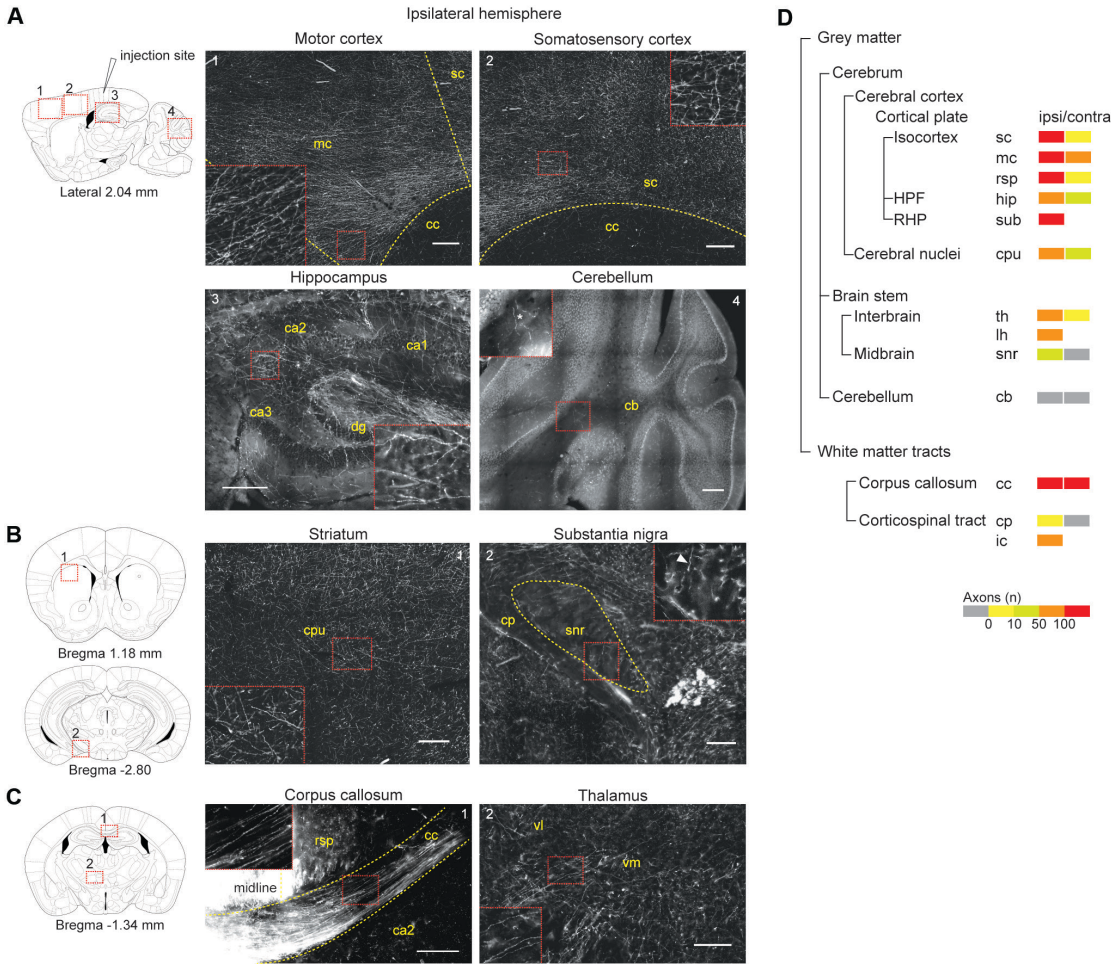

Figure S6. Human neurons project to known SCx1 targets. (**A**), Schematic sagittal view of the adult mouse brain (left). Numbered red boxes indicate: (1) somatosensory cortex adjacent to the injection site, (2) motor cortex, (3) hippocampus, and (4) cerebellum. Representative immunostaining of the numbered regions shown in the schematic for hNCAM (neuronal marker) at 5 mpt (right). Asterisk marks autofluorescence in a vessel. (**B**), Schematic coronal view of the adult mouse brain 1.18 (top left) and -2.80 mm (bottom left) from Bregma. Representative hNCAM immunostaining of the striatum, substantia nigra and cerebral peduncle at 5 mpt (right). Arrowhead in the inset shows an example of axon fiber. (**C**), Schematic coronal view of the adult mouse brain 1.34 mm from Bregma (left). Numbered red boxes indicate: (1) corpus callosum and (2) thalamus. Representative immunostaining of the regions indicated in the schematic for hNCAM at 5 mpt (right). Schematic brain images adapted from Paxinos and Franklin, 2001. Dashed yellow lines mark anatomical boundaries. Red dashed boxes contain magnified insets of images. Scale bars, 200 µm (A, B, C). (**D**), Quantification of axonal density in grey and white matter brain regions (n = 3 animals). Fiber density is color-coded (from grey: no human axons, to bright red: more than 100 human axons). mc, motor cortex; sc, somatosensory cortex; rsp, retrosplenial cortex; HPF, hippocampal formation; hip, hippocampal region; ca1, ca2, ca3 indicate CA1, CA2, CA3 subfields of hippocampus, respectively; dg, dentate gyrus; RHP, retrohippocampal region; sub, subiculum; cpu, caudate-putamen (striatum); th, thalamus; lh, lateral

hypothalamus; snr, substantia nigra; cb, cerebellum; cc, corpus callosum; cp, cerebral peduncle; ic, internal capsule; vl, ventrolateral thalamus; vm, ventromedial thalamus.

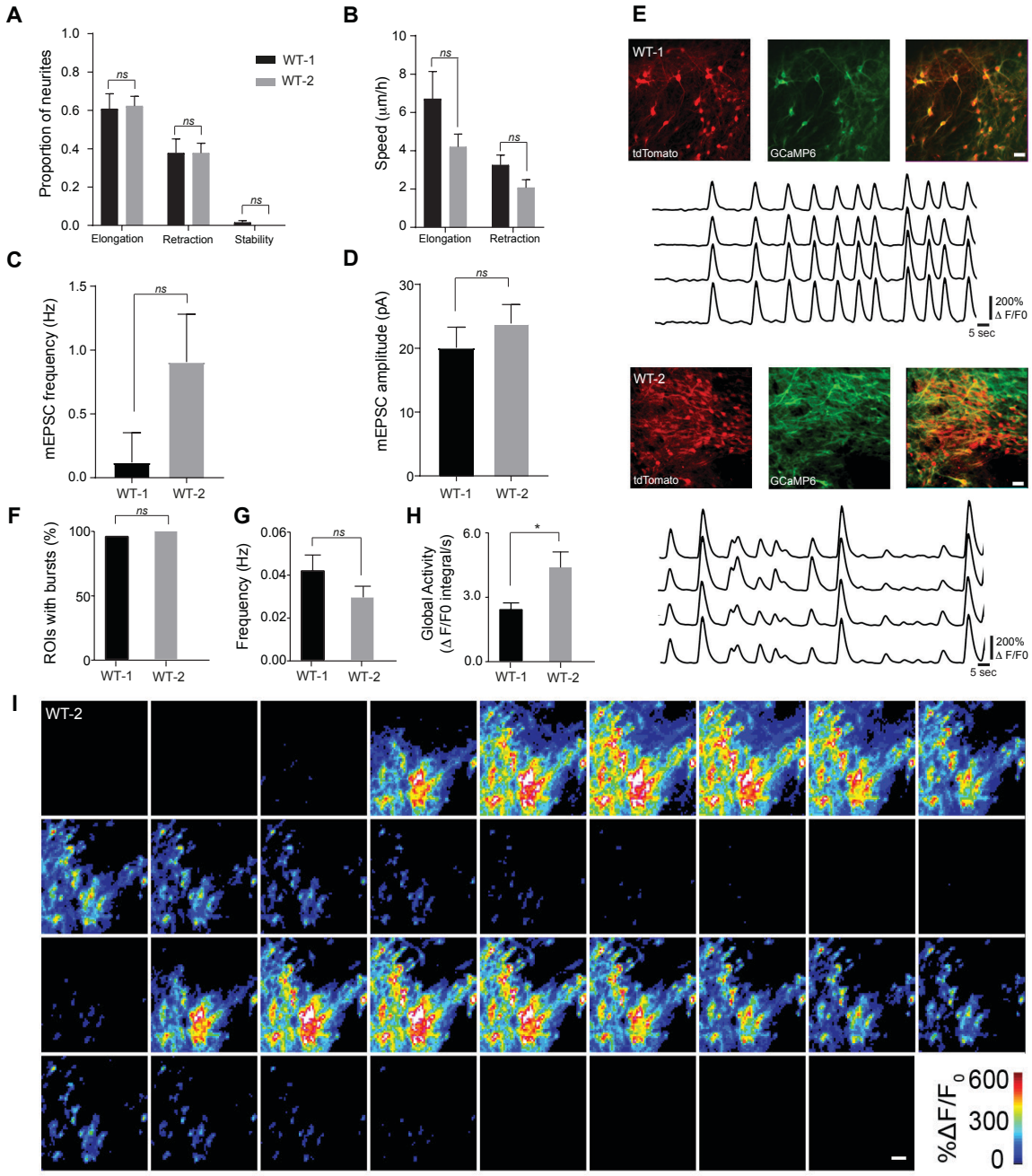

Figure S7. Reproducible human neuron dynamics in cortical tissue grafts from two independent control iPSC lines.

(**A**) Quantification of the proportion of neurites elongating, retracting and stable in 24h intervals at 3 wpt from WT-1 (n = 96 neurites from 79 cells in 7 animals) and WT-2 (n = 65 neurites from 53 cells in 4 animals) grafts. Unpaired two-tailed t-test, P = 0.2401 (elongation), P = 0.0510 (retraction). (**B**) Quantification of the speed of neurite elongation and retraction at 3 wpt in WT-1 (n = 96 neurites from 73 cells in 7 animals) and WT-2 grafts (n = 53 neurites from 43 cells in 4 animals). Two-way ANOVA, interaction $F_{6,54}$ = 0.3626, P = 0.8993. (**C**, **D**) Frequency and amplitude of mEPSC recorded at 5 mpt in WT-1 (n =18 cells from 4 animals) and WT-2 (n = 23 cells from 4 animals) grafts. Unpaired two-tailed t-test, P = 0.4237 (amplitude). Mann-Whitney U-

test, $P = 0.8812$ (frequency). (**E**) Example of burst activity and representative $\Delta F/F_0$ calcium traces from 4 active neurons in WT-1 and WT-2 grafts. Scale bar, 20 µm. (**F**) Percentage of ROIs in WT-1 (49/51 ROIs, 96 %) and WT-2 (33/33 ROIs, 100 %) grafts exhibiting spontaneous bursting activity. Z-test, $P = 0.662$. (**G**) Frequency of burst events in WT-1 and WT-2 at 3-5 months. Mann-Whitney *U*-test, $P = 0.376$. (**H**) Global activity for WT-1 vs WT-2 grafts at 3-5 months. Mann-Whitney U-test, $^*P < 0.05$. (**I**) Montage of image frames from a typical recurrent burst in a WT-2 graft at 112 dpt. Montage taken from movie S5. Scale bar 20 µm. Data are represented as mean ± SEM. *ns*, not significant.

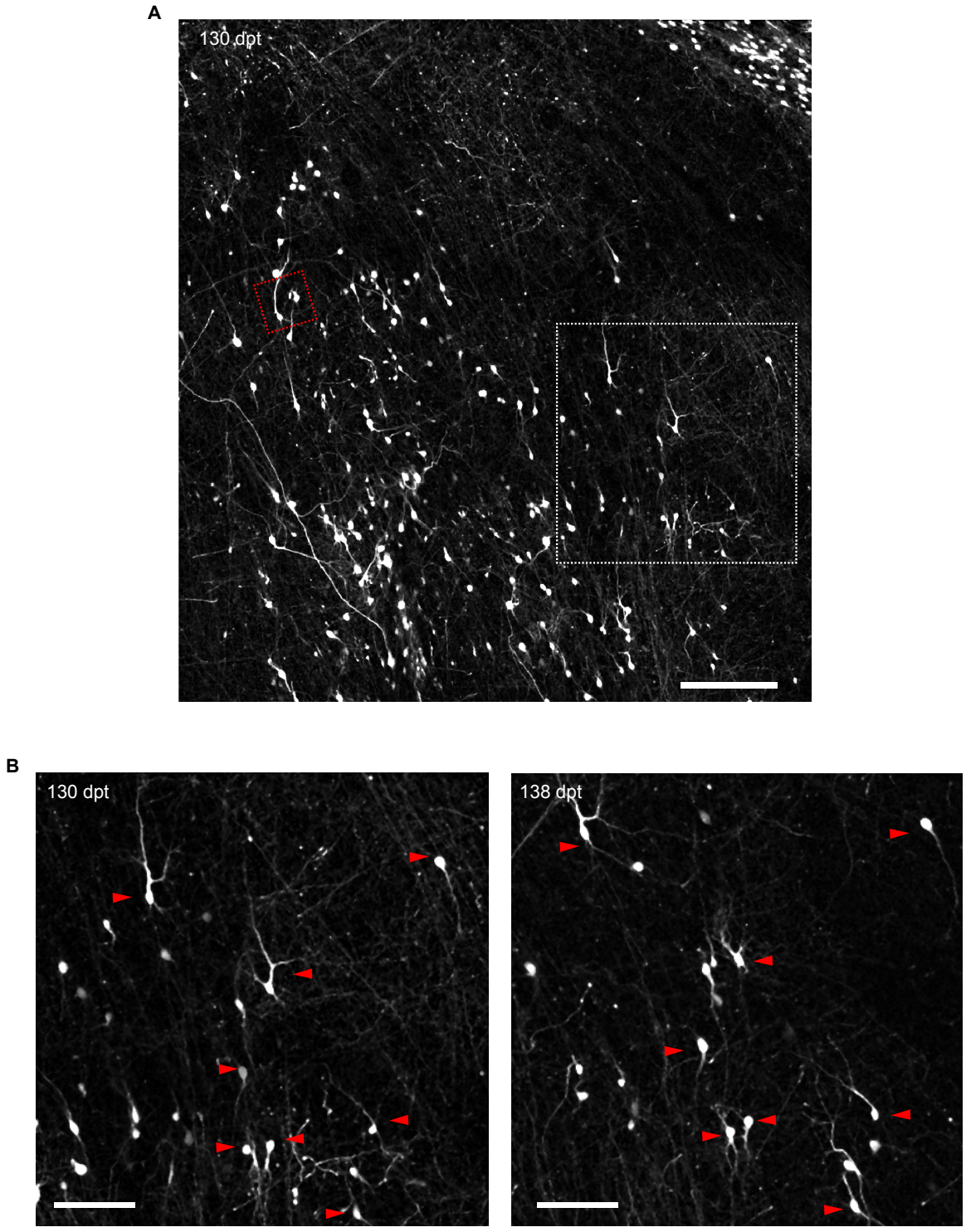

Figure S8. *In vivo* tracking of transplanted WT human neurons over 8 days.
(**A**) 2-photon *in vivo* imaging of a WT-1 graft at 130 dpt. Red box indicate same area as in fig. 2B, top panel. Scale bar, 200 µm. (**B**) Imaging of the same graft area (white box in (A)) over the indicated time. Red arrows represent examples of cells with a stable location over a 8-day period. Scale bars, 100 µm.

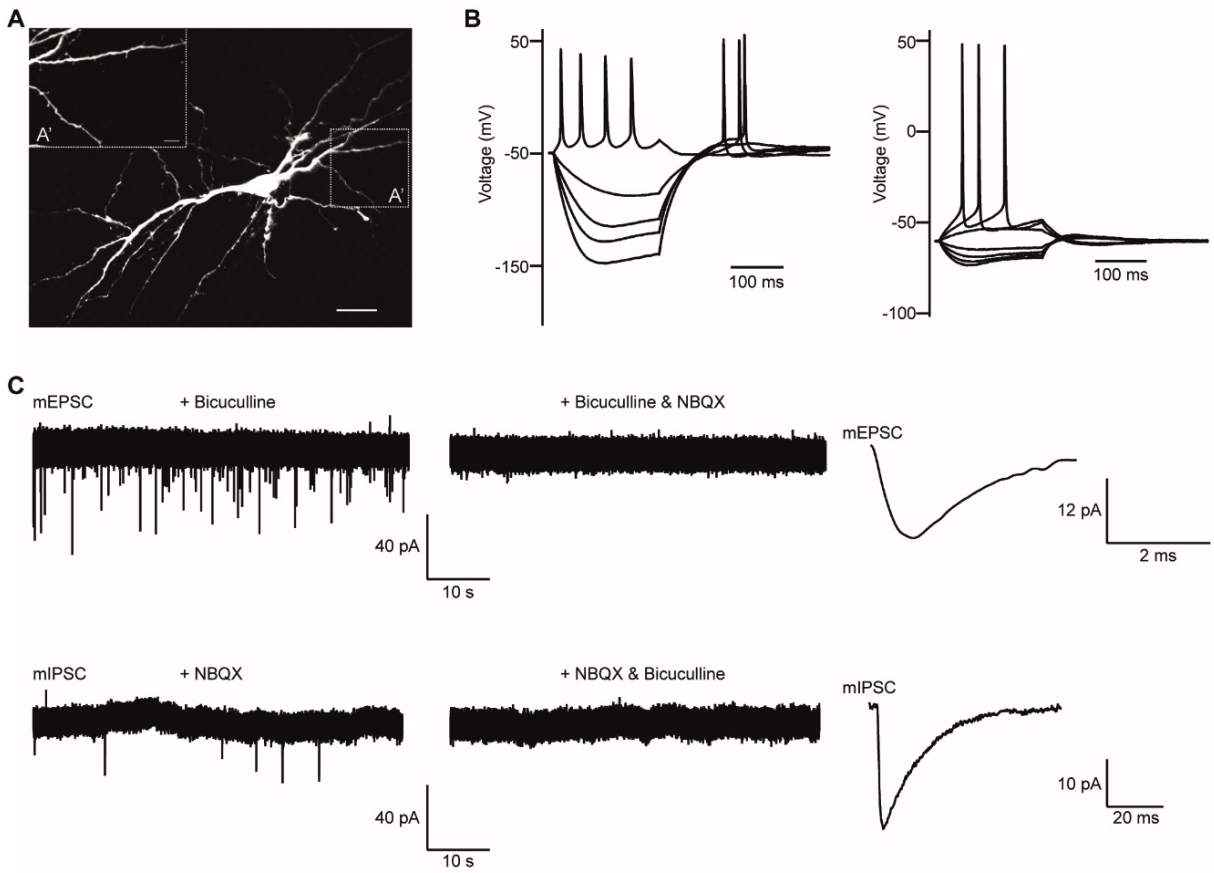

Figure S9. Excitability and functional synaptic connections in control human tissue grafts. (**A**) Representative example of a Lucifer yellow-filled human pyramidal neuron. (**B**) Two examples of current-voltage relationships of two pyramidal shaped GFP-positive human iPSC-derived neurons in human grafts. Potentials are evoked by 200 ms pulses from -80 to +50 pA. (**C**) Top, representative spontaneous miniature excitatory synaptic currents (mEPSC, downward deflections) recorded in voltage-clamp (-70 mV) in the absence (left) and presence of NBQX (5 µM, middle). Mean ensembled mEPSCs from 60 events captured from a single neuron is shown on the right at an expanded time scale. Bottom, spontaneous miniature inhibitory synaptic currents (mIPSC, downward deflections) recorded in symmetrical chloride conditions and in the presence of NBQX (5 µM, left). mIPSC are completely blocked by (+)-bicuculline (middle, 20 µM). Mean ensembled mIPSCs for 40 events from a single neuron is shown on the right at an expanded time scale.

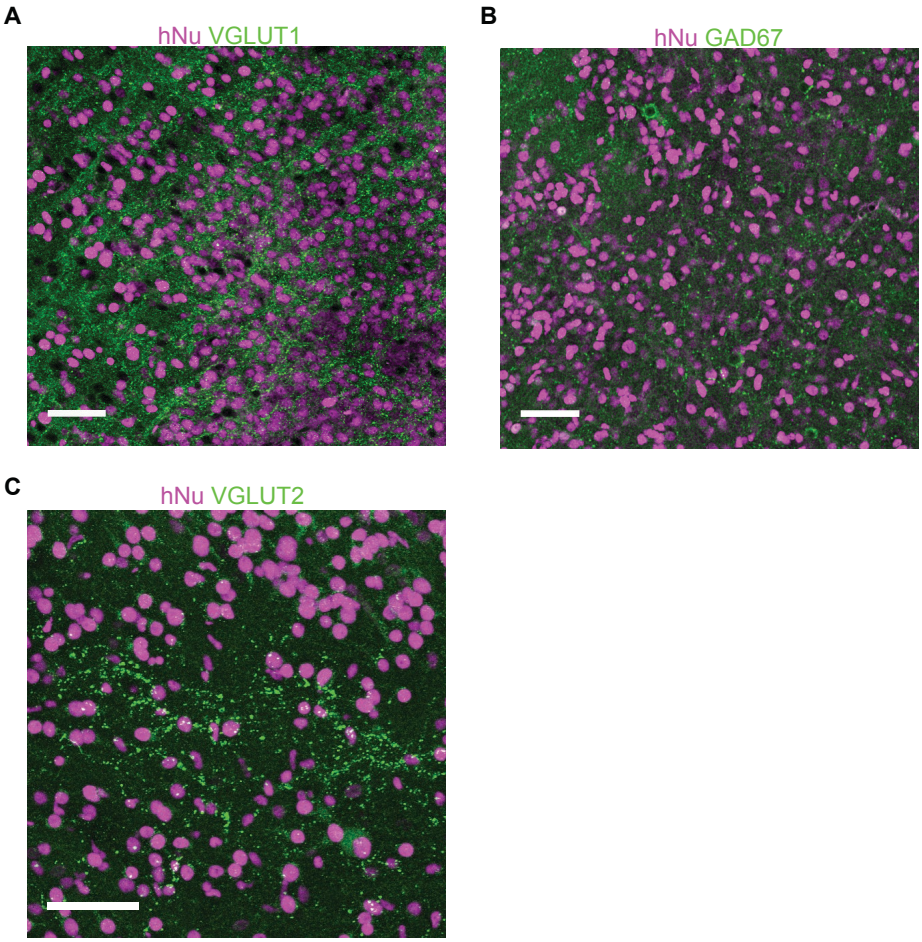

Figure S10. Human grafts contain glutamatergic, GABAergic and thalamocortical terminals. (**A**) Representative example (single plane) of a WT-1 graft stained for Vesicular glutamate transporter 1 (VGLUT1, a marker for excitatory presynaptic terminals; *n* = 2 grafts, at 5 mpt). (**B**) Representative example (single plane) of a WT-1 graft stained for GAD67 (*n* = 3 grafts, at 5 mpt). (**C**) Representative maximum intensity projection (34 planes, 0.5 µm step size) from a WT-2 graft stained for VGLUT2 (a marker for thalamocortical presynaptic terminals) (*n* = 3 grafts at 6 mpt). Scale bars, 50 µm.

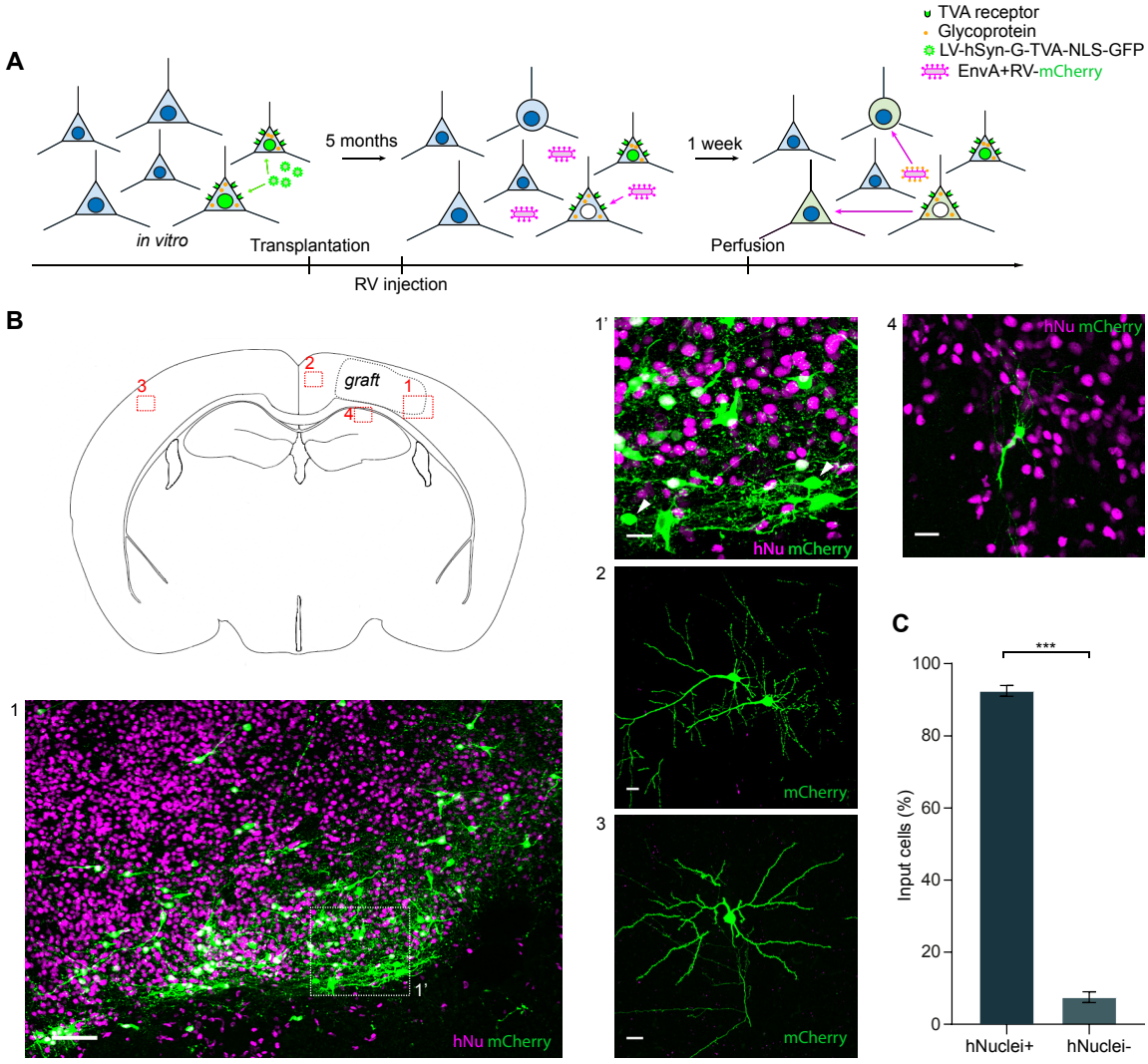

Figure S11. Other human neurons and a small proportion of host neurons are the source of synaptic input. (**A**), Experimental design of retrograde monosynaptic tracing of human neurons with ΔG-rabies virus. (**B**), Location of host input cells in the periphery of the graft (1, 1'), ipsilateral cortex (2), contralateral cortex (3), and in the CA1 region of the ipsilateral hippocampus (4). (**C**), Quantification of human versus host input cells (n = 2 animals, unpaired t-test, ***$P < 0.001$). Scale bars, 100 µm (1) and 20 µm (1', 2, 3, 4).

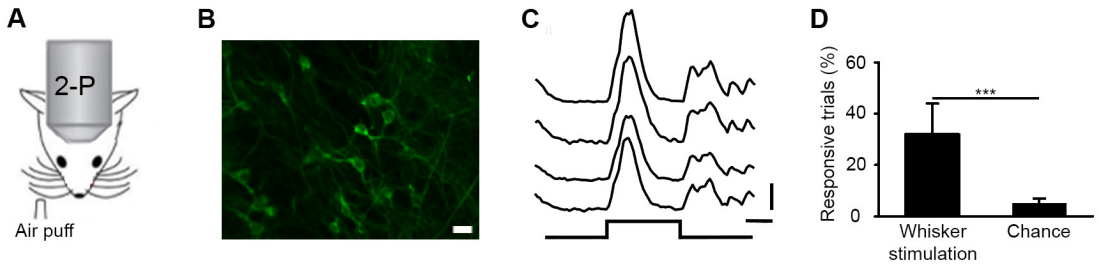

Figure S12. Sensory-evoked activity in human tissue grafts.
(**A**), Cartoon of SCx1 imaging paradigm for whisker stimulation showing mouse under 2P microscope and contralateral whisker stimulation via air puffs. Whisker stimulation was delivered as 8 pulses in 4 trains delivered over 10 seconds. (**B**), Example of imaged cortical regions taken from a WT-1 graft in the Scx1 of an adult mouse. GCaMP6s positive neurons are shown as a maximum intensity projection of activity over a 4 – 5 min period of sensory evoked activity. (**C**), Example of $\%\Delta F/F_0$ calcium traces in response to whisker stimulation for 4 active neurons. Responses are the average of 5 trials. (**D**), Percentage of trials defined as responsive (see methods) during periods with either whisker stimulation (32 ± 12 %, n = 5 regions and 25 trials from one mouse) or with no sensory stimulation (5 ± 2 %, n = 20 regions and 100 trials from 3 mice). Trials without whisker stimulation were used to define the chance levels of measuring a false positive response. The percentage of responsive trials was greater with whisker stimulation (unpaired t-test, $P < 0.001$,). Error bars are mean and s.e.m. Scale bars, 20 µm (**B**), 10 s and 100 % $\Delta F/F_0$ (**C**). The data in this figure is taken from 25 cortical regions across 4 animals.

Marker	Chromo-some	Allele	WT-1	Ts21-1	Ts21 fibro-blast	Ts21-2	WT-2	WT-2’
TPOX	2	1 2						
D3S1358	3	1 2						
FGA	4	1 2	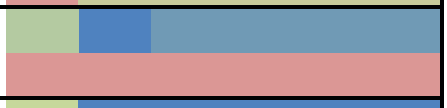					
CSF1PO	5	1 2						
D5S818	5	1 2	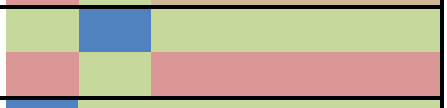					
D7S820	7	1 2						
D8S1179	8	1 2						
TH01	11	1 2						
vWA	12	1 2						
D13S317	13	1 2	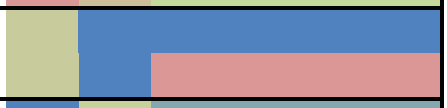					
Penta E	15	1 2						
D16S539	16	1 2	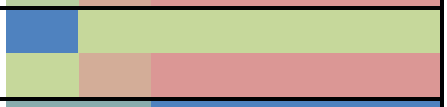					
D18S51	18	1 2						
D21S11	21	1 2 3	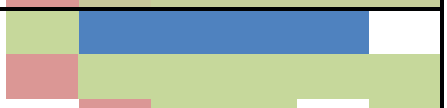					
Penta D	21	1 2 3	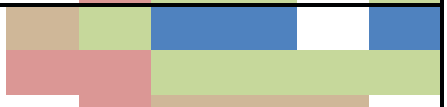					
AMEL	XY	x y	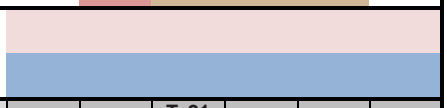					

Figure S13. iPSC-line identity verification. Microsatellite short tandem repeat (STR) assay for WT-1, Ts21-1, WT-2, Ts21-2 iPS cell lines together with the Ts21 fibroblasts, the originating fibroblast lines for the trisomic/revertant disomic pair, and WT-2', a further clone showing spontaneous loss of chromosome 21. Within each locus, varying repeat lengths are discriminated by alternate color. Note that the parental fibroblasts and Ts21-2 are both trisomic for Hsa21 and identical to each other, and that WT-2 and WT-2' are both disomic for different pairs of Hsa21, but otherwise identical to the fibroblasts and Ts21-2.

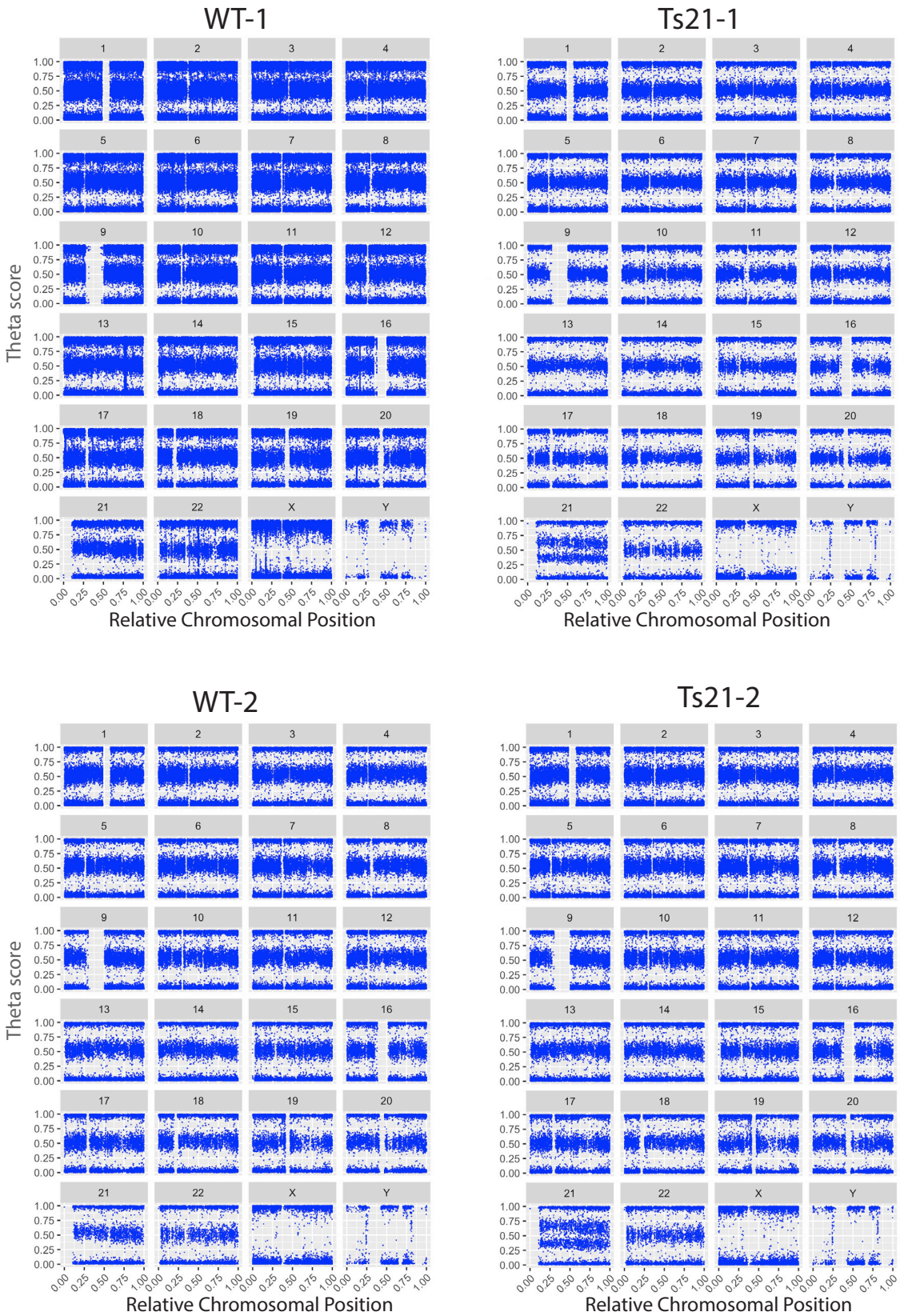

Figure S14. Genome-wide copy number SNP assay. Molecular karyotyping analysis with genome-wide copy number single nucleotide polymorphism (SNP) assay showing

Theta scores (allelic SNP ratio) for individual SNP loci (vertical axis) against normalized distance along chromosome (horizontal axis). Note no major genomic deletions or duplications and expected Ts21 in Ts21-1 and Ts21-2, and euploidy in WT-1 and WT-2.

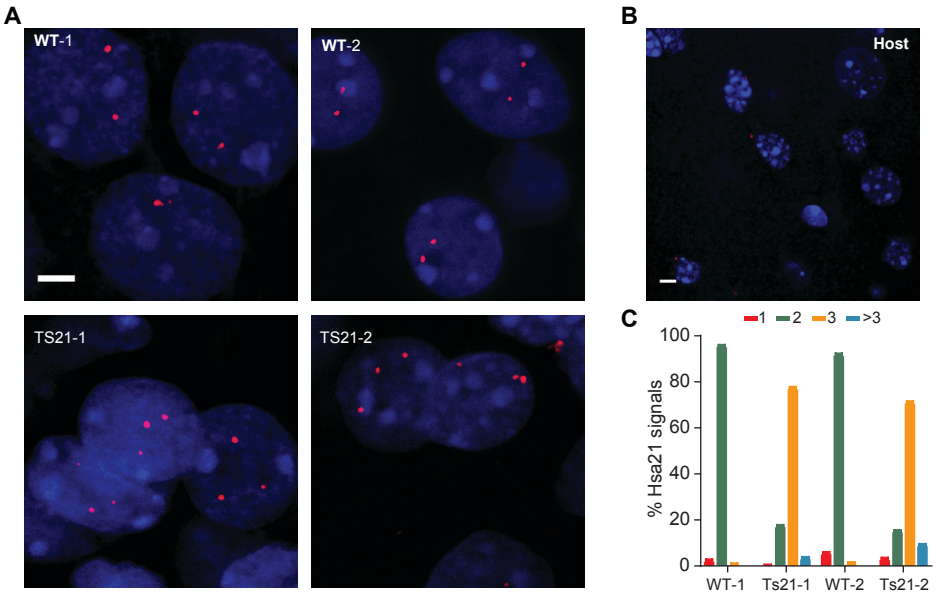

Figure S15. Fluorescent In Situ Hybridization assay (FISH). (**A**) Representative examples of Hsa21-specific FISH signal (red), in each of the four transplanted lines at 5 mpt. Nuclei are counterstained for Dapi (blue). Scale bar, 3 µm. (**B**) Representative example from the host contralateral cortex (negative control). Scale bar, 5 µm. (**C**) Quantification confirming the expected number of XL 21q22 copies in the human tissue grafts from each of the four lines.

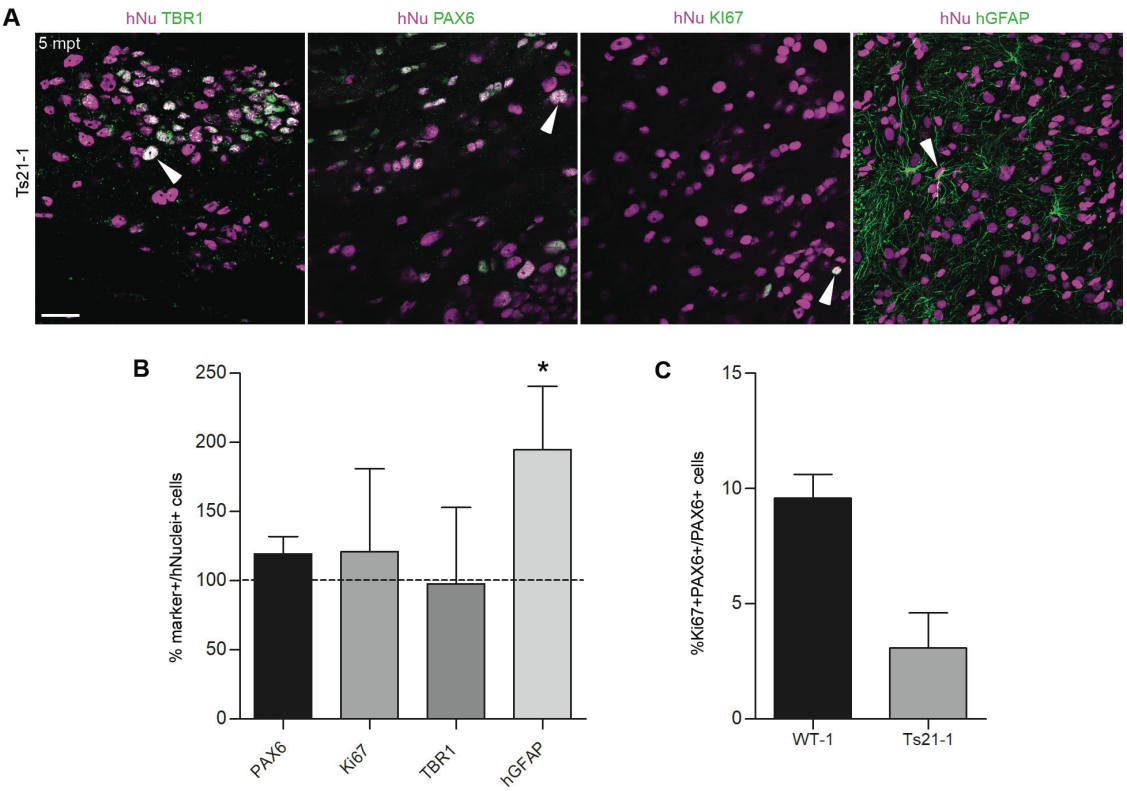

Figure S16. Similar proportion of progenitors, neurons and proliferating cells but increased astroglia in Ts21 human tissue grafts compared to control. (**A**) Representative immunostaining of human Ts21-1 cortical graft for TBR1, PAX6, KI67 and human GFAP at 5 mpt; arrowheads indicate examples positive human cells. Scale bar, 30 µm. (**B**) Relative percentage of Ts21 cell populations *in vivo* ($n = 3$ animals) at 5 mpt (area sampled per cell marker: 1.42 ± 0.76, mean ± SD), normalized to control values (dotted line; area sampled per cell marker: 0.94 ± 0.11, mean ± SD). Unpaired two-tailed *t*-test, $*P < 0.05$. (**C**) Proportion of proliferating PAX6-expressing progenitor cells in WT-1 and Ts21-1 lines at 5 mpt ($n = 2$ mice each line; area sampled: 2.46 ± 0.60 and 1.82 ± 0.18 respectively, mean ± SD). Mann-Whitney U-test, $P = 0.333$.

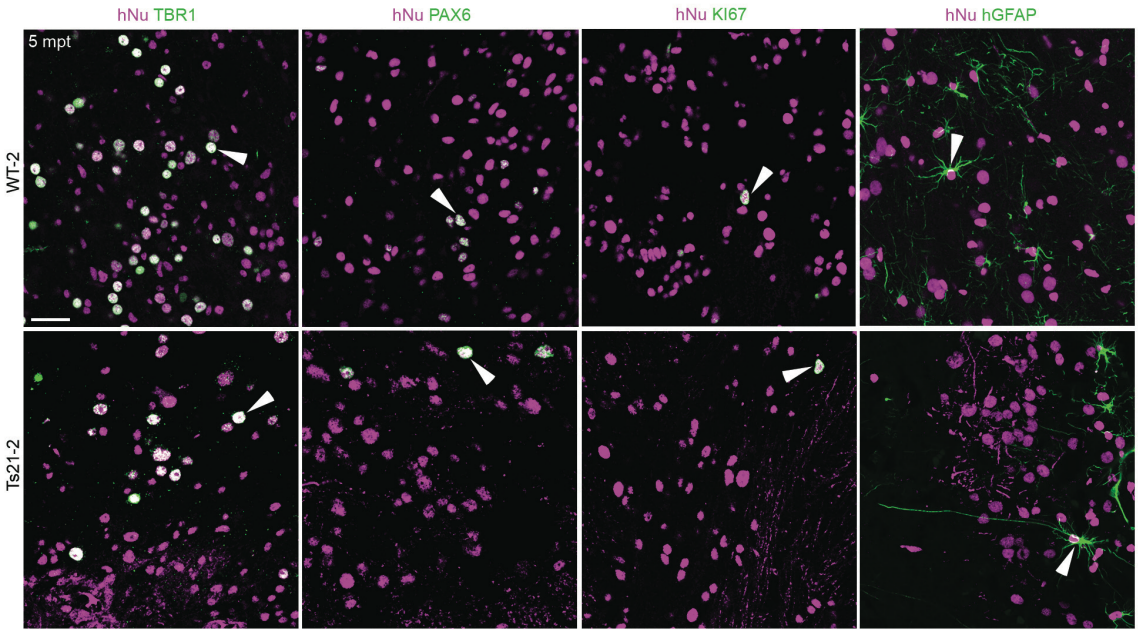

Figure S17. WT-2 and Ts21-2 graft cell identity. Representative immunostaining of human WT-2 and Ts21-2 grafts for TBR1, PAX6, Ki67 and human GFAP at 5 mpt. Arrowheads show examples of positive human cells. Scale bar, 30 µm.

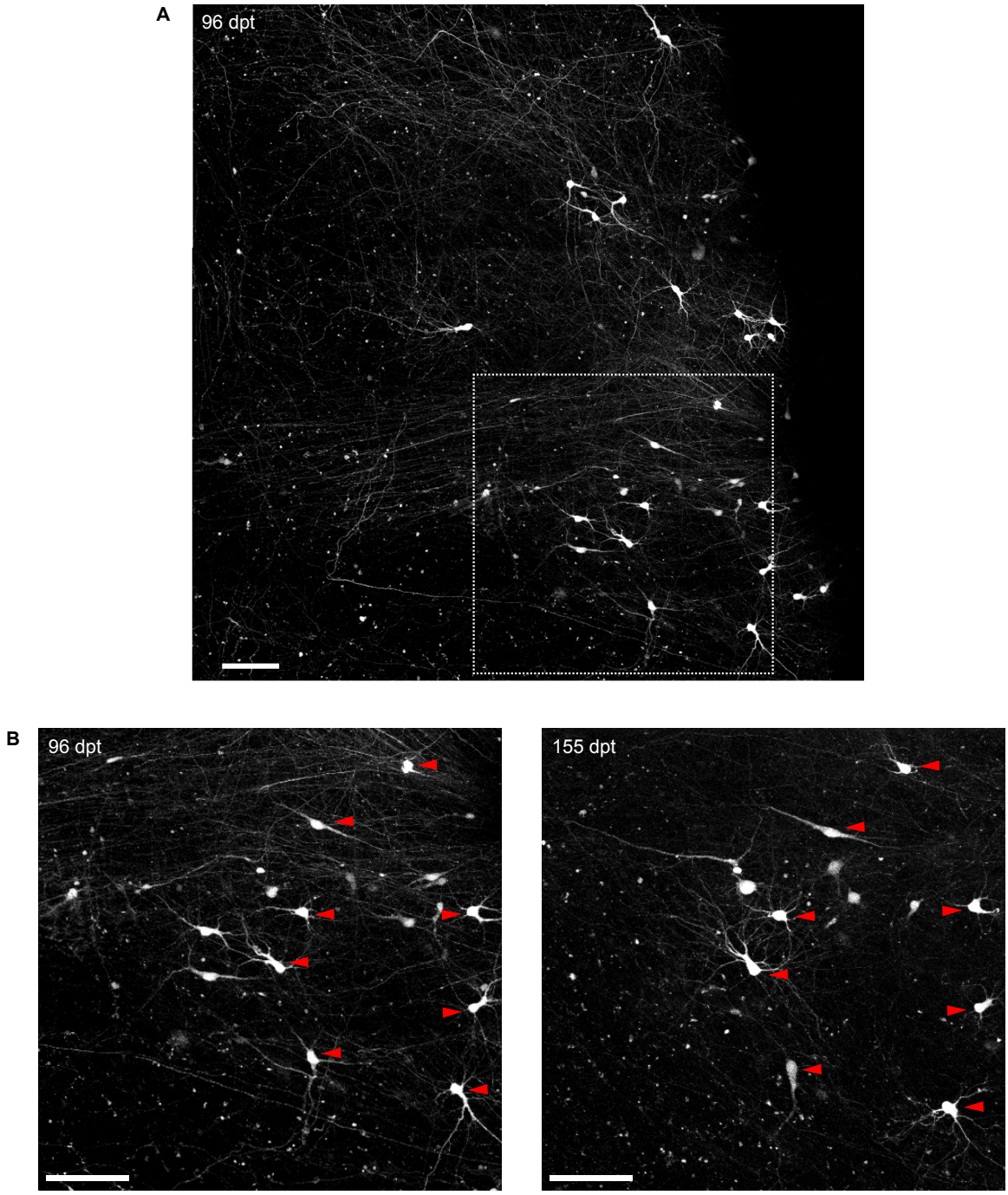

Figure S18. *In vivo* tracking of transplanted Ts21 human neurons over 2 months. (**A**) 2-photon *in vivo* imaging of a Ts21-1 graft at 96 dpt. Scale bar, 100 µm. (**B**) 2-photon *in vivo* imaging of the same graft area (white box in (A)) over the indicated time. Red arrows represent examples of cells with a stable location over a 2-month period. Scale bars, 100 µm.

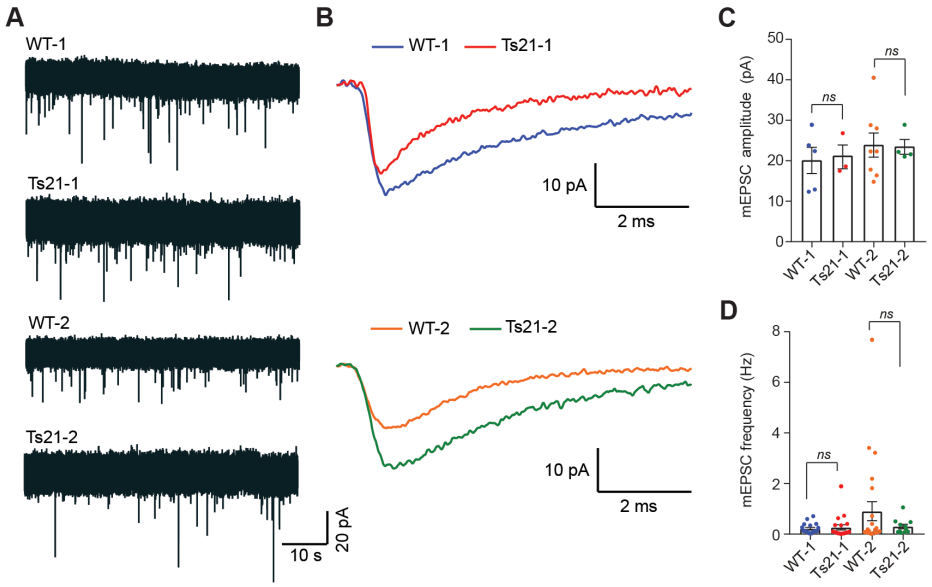

Figure S19. Similar synaptic input in Ts21 neurons compared to control. (**A**) Representative traces of mEPSC recorded in voltage-clamp mode (-70 mV) from WT-1/2 and Ts21-1/2 grafts at 5 mpt. (**B**) Expanded traces of mEPSC shown in A. (**C**, **D**), mEPSC amplitude (WT-1, $n = 5$; Ts21-1, $n = 3$; WT-2, $n = 8$ and Ts21-2, $n = 4$) and frequency (WT-1, $n = 18$; Ts21-1, $n = 19$ cells; WT-2, $n = 23$ and Ts21-2, $n = 11$) in cortical tissue grafts from 3 mice each. Kruskal-Wallis test: amplitude, $P = 0.8395$; frequency, $P = 0.2094$. Each data point represents a cell. *ns*, not significant.

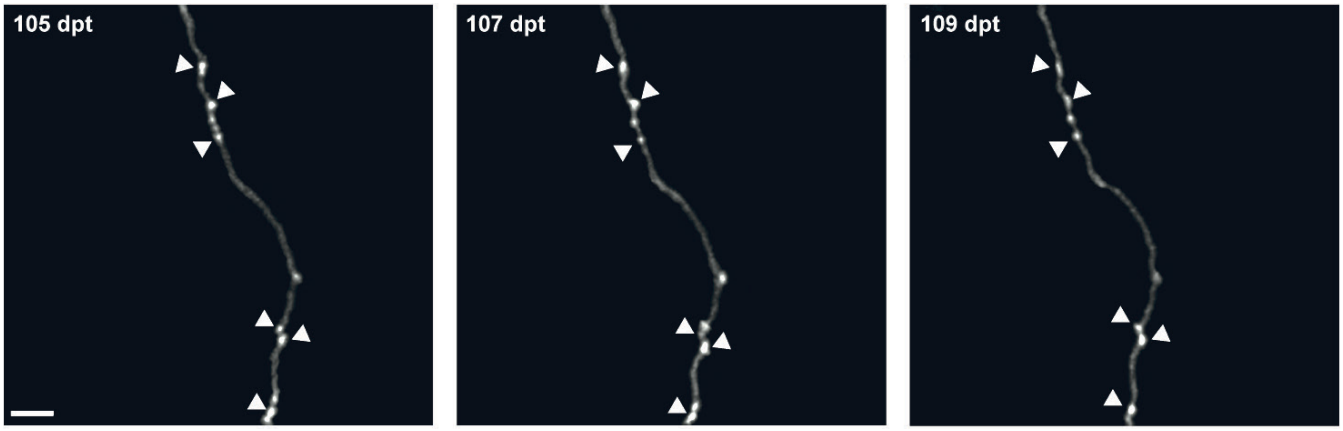

Figure S20. 2-photon *in vivo* imaging of EPB stability on Ts21 neurons. Example of stable EPBs (arrowheads) on Ts21 neurons *in vivo* over the indicated time points. Scale bar, 5 μm.

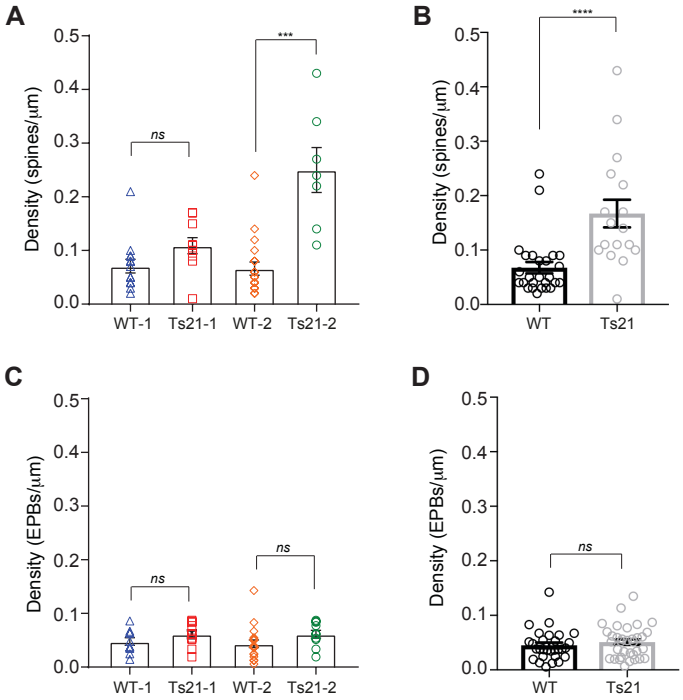

Figure S21. Spine and bouton density in cortical tissue grafts. (**A**) Dendritic spine density at Day 0 in WT-1 (n = 14 cells from 3 animals), Ts21-1 (n = 10 cells from 4 animals), WT-2 (n = 12 cells from 4 animals) and Ts21-2 (n = 7 cells from 2 animals) grafts at 3-4 mpt. Kruskal-Wallis test, ***$P < 0.001$; *ns*, not significant. Each data point represents a cell. (**B**) Dendritic spine density at Day 0 in WT-1/2 (n = 26 cells from 7 animals) and Ts21-1/2 (n = 17 cells from 6 animals) grafts at 3-4 mpt. Mann-Whitney test, ****$P < 0.0001$. Each data point represents a cell. (**C**) EPB density at Day 0 in WT-1 (n = 10 cells from 3 animals), Ts21-1 (n = 10 cells from 3 animals), WT-2 (n = 19 cells from 4 animals) and Ts21-2 (n = 10 cells from 3 animals) in grafts at 3-4 mpt. Kruskal-Wallis test; *ns*, not significant. Each data point represents a cell. (**D**) EPB density at Day 0 in WT-1/2 (n = 29 cells from 7 animals) and Tss21-1/2 (n = 20 cells from 6 animals) in grafts at 3-4 mpt. Mann-Whitney test; *ns*, not significant. Each data point represents a cell.

Table S1.

List of Antibodies.

Antibody	Host Species	Dilution	Reference
Human Nestin (cl. 196908)	Mouse monoclonal	1:1000	R&D Systems, MAB1259
PDFG Receptor α	Rabbit	1:1000	Cell Signaling, 3164
GFP	Chicken	1:300	Novus Biologicals, NB100-1614
Doublecortin	Rabbit	1:400	Cell Signaling, 4604
Ki67	Rabbit	1:1000	Abcam, ab15580
Ki67 (clone B56)	Mouse monoclonal	1:100	BD Biosciences, 550609
Ki67 [OTI5D7]	Rat monoclonal	1:500	Abcam, ab156956
Human Nuclei	Mouse monoclonal	1:200	Millipore, MAB1281
Pax-6	Rabbit	1:300	Biolegend, 901301
NuMA	Rabbit	1:200	Abcam, ab97585
NCAM (ERIC-1)	Mouse monoclonal	1:1000	Santa Cruz Biotechnology, sc-106
Human GFAP	Mouse monoclonal	1:500	Stem123, AB-123-U-050
GFAP	Rabbit	1:1000	DAKO, Z0334
GAD67	Rabbit	1:500	Abcam, ab97739
Iba1	Goat	1:1000	Abcam, ab5076
CD31	Rat	1:200	Biolegend, 102402
TBR1	Rabbit	1:200	Abcam, ab31940
SATB2 [SATBA4B10]	Mouse monoclonal	1:200	Abcam, ab51502
β-actin	Mouse	1:10000	Sigma, A228
APP C-Terminal Fragment	Mouse	1:1000	Biolegend, 802801
TuJ1	Rabbit and Mouse	1:5000	Biolegend, 802001 and 8012021
Synapsin1	Rabbit	1:1000	Abcam, ab8
PSD95	Rabbit	1:1000	Abcam, ab18258
CTIP2 [25B6]	Rat monoclonal	1:300	Abcam, ab18465
OLIG2	Rabbit	1:1000	Millipore, AB9610
VGLUT1	Guinea Pig	1:1000	Millipore, AB5905
VGLUT2	Guinea Pig	1:2000	Synaptic sys., 135-404
DsRed	Rabbit	1:500	Clontech, 632496

Movie S1

Example of WT-1 tissue graft stained for human Neural Cell Adhesion Molecule (NCAM), a human neuron specific antibody, at 5 mpt.

Movie S2

Example of axonal bundles (arrowheads) and vessels (asterisks) in a cortical tissue graft imaged *in vivo* at 3 mpt. Scale bar 50 μm.

Movie S3

Example of axonal layers in a cortical tissue graft imaged *in vivo* at 102 dpt. A montage representation of this 2-photon z-stack is shown in fig. 1F. Scale bar 50 μm.

Movie S4

Example of time series of WT-1 GCaMP6s-expressing human neurons in the adult somatosensory cortex at 5 mpt. Movie was acquired at 3 Hz and is shown at 6 fps. Scale bar, 50 μm.

Movie S5

Example of time series of WT-2 GCaMP6s-expressing human neurons showing stereotypical patterns of population activity *in vivo* at 112 dpt. Movie was acquired at 3 Hz and is shown at 6 fps. A montage representation of this time series is shown in fig. S7I. Scale bar, 50 μm.

Movie S6

Example of time series of Ts21-1 GCaMP6s-expressing human neurons in the adult somatosensory cortex at 5 mpt. Movie was acquired at 3 Hz and is shown at 6 fps. Scale bar, 50 μm.

References

1. W. M. Cowan, J. W. Fawcett, D. D. O'Leary, B. B. Stanfield, Regressive events in neurogenesis. *Science* **225**, 1258-1265 (1984).
2. L. K. Low, H. J. Cheng, Axon pruning: an essential step underlying the developmental plasticity of neuronal connections. *Philos Trans R Soc Lond B Biol Sci* **361**, 1531-1544 (2006).
3. Y. Herault *et al.*, Rodent models in Down syndrome research: impact and future opportunities. *Disease models & mechanisms* **10**, 1165-1186 (2017).
4. A. O'Doherty *et al.*, An aneuploid mouse strain carrying human chromosome 21 with Down syndrome phenotypes. *Science* **309**, 2033-2037 (2005).
5. M. Gupta, A. R. Dhanasekaran, K. J. Gardiner, Mouse models of Down syndrome: gene content and consequences. *Mamm Genome* **27**, 538-555 (2016).
6. I. Espuny-Camacho *et al.*, Hallmarks of Alzheimer's Disease in Stem-Cell-Derived Human Neurons Transplanted into Mouse Brain. *Neuron* **93**, 1066-1081 e1068 (2017).
7. J. van den Ameele, L. Tiberi, P. Vanderhaeghen, I. Espuny-Camacho, Thinking out of the dish: what to learn about cortical development using pluripotent stem cells. *Trends Neurosci* **37**, 334-342 (2014).
8. Y. Shi, P. Kirwan, J. Smith, H. P. Robinson, F. J. Livesey, Human cerebral cortex development from pluripotent stem cells to functional excitatory synapses. *Nat Neurosci* **15**, 477-486, S471 (2012).
9. M. A. Lancaster *et al.*, Cerebral organoids model human brain development and microcephaly. *Nature* **501**, 373-379 (2013).
10. P. Carmeliet, M. Tessier-Lavigne, Common mechanisms of nerve and blood vessel wiring. *Nature* **436**, 193-200 (2005).
11. L. H. Thompson, A. Bjorklund, Reconstruction of brain circuitry by neural transplants generated from pluripotent stem cells. *Neurobiol Dis* **79**, 28-40 (2015).
12. J. S. Barbosa *et al.*, Neurodevelopment. Live imaging of adult neural stem cell behavior in the intact and injured zebrafish brain. *Science* **348**, 789-793 (2015).
13. Y. Shi, P. Kirwan, F. J. Livesey, Directed differentiation of human pluripotent stem cells to cerebral cortex neurons and neural networks. *Nat Protoc* **7**, 1836-1846 (2012).
14. M. E. Emborg *et al.*, Induced pluripotent stem cell-derived neural cells survive and mature in the nonhuman primate brain. *Cell reports* **3**, 646-650 (2013).
15. X. Qian *et al.*, Brain-Region-Specific Organoids Using Mini-bioreactors for Modeling ZIKV Exposure. *Cell* **165**, 1238-1254 (2016).
16. A. Hoerder-Suabedissen, Z. Molnar, Development, evolution and pathology of neocortical subplate neurons. *Nat Rev Neurosci* **16**, 133-146 (2015).
17. T. Saito *et al.*, Neocortical layer formation of human developing brains and lissencephalies: consideration of layer-specific marker expression. *Cereb Cortex* **21**, 588-596 (2011).
18. N. Palomero-Gallagher, K. Zilles, Cortical layers: Cyto-, myelo-, receptor- and synaptic architecture in human cortical areas. *Neuroimage*, (2017).
19. I. M. Zakiewicz, J. G. Bjaalie, T. B. Leergaard, Brain-wide map of efferent projections from rat barrel cortex. *Front Neuroinform* **8**, 5 (2014).

20. I. Espuny-Camacho *et al.*, Pyramidal neurons derived from human pluripotent stem cells integrate efficiently into mouse brain circuits in vivo. *Neuron* **77**, 440-456 (2013).
21. L. Luo, D. D. O'Leary, Axon retraction and degeneration in development and disease. *Annu Rev Neurosci* **28**, 127-156 (2005).
22. A. Nikolaev, T. McLaughlin, D. D. O'Leary, M. Tessier-Lavigne, APP binds DR6 to trigger axon pruning and neuron death via distinct caspases. *Nature* **457**, 981-989 (2009).
23. C. Portera-Cailliau, R. M. Weimer, V. De Paola, P. Caroni, K. Svoboda, Diverse modes of axon elaboration in the developing neocortex. *PLoS Biol* **3**, e272 (2005).
24. V. De Paola *et al.*, Cell type-specific structural plasticity of axonal branches and boutons in the adult neocortex. *Neuron* **49**, 861-875 (2006).
25. V. De Paola, S. Arber, P. Caroni, AMPA receptors regulate dynamic equilibrium of presynaptic terminals in mature hippocampal networks. *Nat Neurosci* **6**, 491-500. (2003).
26. P. Caroni, F. Donato, D. Muller, Structural plasticity upon learning: regulation and functions. *Nat Rev Neurosci* **13**, 478-490 (2012).
27. T. L. Petit, J. C. LeBoutillier, D. P. Alfano, L. E. Becker, Synaptic development in the human fetus: a morphometric analysis of normal and Down's syndrome neocortex. *Exp Neurol* **83**, 13-23 (1984).
28. P. R. Huttenlocher, A. S. Dabholkar, Regional differences in synaptogenesis in human cerebral cortex. *J Comp Neurol* **387**, 167-178 (1997).
29. M. E. Molliver, I. Kostovic, H. van der Loos, The development of synapses in cerebral cortex of the human fetus. *Brain Res* **50**, 403-407 (1973).
30. A. Holtmaat *et al.*, Long-term, high-resolution imaging in the mouse neocortex through a chronic cranial window. *Nat Protoc* **4**, 1128-1144 (2009).
31. O. Garaschuk, J. Linn, J. Eilers, A. Konnerth, Large-scale oscillatory calcium waves in the immature cortex. *Nat Neurosci* **3**, 452-459 (2000).
32. R. Khazipov, H. J. Luhmann, Early patterns of electrical activity in the developing cerebral cortex of humans and rodents. *Trends Neurosci* **29**, 414-418 (2006).
33. P. Kirwan *et al.*, Development and function of human cerebral cortex neural networks from pluripotent stem cells in vitro. *Development* **142**, 3178-3187 (2015).
34. G. Quadrato *et al.*, Cell diversity and network dynamics in photosensitive human brain organoids. *Nature* **545**, 48-53 (2017).
35. T. W. Chen *et al.*, Ultrasensitive fluorescent proteins for imaging neuronal activity. *Nature* **499**, 295-300 (2013).
36. S. Vanhatalo *et al.*, DC-EEG discloses prominent, very slow activity patterns during sleep in preterm infants. *Clin Neurophysiol* **113**, 1822-1825 (2002).
37. P. J. Uhlhaas, F. Roux, E. Rodriguez, A. Rotarska-Jagiela, W. Singer, Neural synchrony and the development of cortical networks. *Trends Cogn Sci* **14**, 72-80 (2010).
38. A. A. Mansour *et al.*, An in vivo model of functional and vascularized human brain organoids. *Nat Biotechnol*, (2018).
39. C. Chen *et al.*, Role of astroglia in Down's syndrome revealed by patient-derived human-induced pluripotent stem cells. *Nature communications* **5**, 4430 (2014).

40. G. A. Maclean *et al.*, Altered hematopoiesis in trisomy 21 as revealed through in vitro differentiation of isogenic human pluripotent cells. *Proc Natl Acad Sci U S A* **109**, 17567-17572 (2012).
41. J. P. Weick *et al.*, Deficits in human trisomy 21 iPSCs and neurons. *Proc Natl Acad Sci U S A* **110**, 9962-9967 (2013).
42. K. Plona, T. Kim, K. Halloran, A. Wynshaw-Boris, Chromosome therapy: Potential strategies for the correction of severe chromosome aberrations. *Am J Med Genet C Semin Med Genet* **172**, 422-430 (2016).
43. E. Dossi, F. Vasile, N. Rouach, Human astrocytes in the diseased brain. *Brain research bulletin* **136**, 139-156 (2018).
44. K. Mollgard, J. J. Lundberg, B. K. Beebe, A. Bjorklund, U. Stenevi, The intracerebrally cultured 'microbrain': a new tool in developmental neurobiology. *Neurosci Lett* **8**, 295-301 (1978).
45. S. Falkner *et al.*, Transplanted embryonic neurons integrate into adult neocortical circuits. *Nature* **539**, 248-253 (2016).
46. J. A. Korecka, S. Levy, O. Isacson, In vivo modeling of neuronal function, axonal impairment and connectivity in neurodegenerative and neuropsychiatric disorders using induced pluripotent stem cells. *Mol Cell Neurosci* **73**, 3-12 (2016).
47. D. Tornero *et al.*, Synaptic inputs from stroke-injured brain to grafted human stem cell-derived neurons activated by sensory stimuli. *Brain* **140**, 692-706 (2017).
48. P. Lu *et al.*, Long-distance growth and connectivity of neural stem cells after severe spinal cord injury. *Cell* **150**, 1264-1273 (2012).
49. V. Tabar *et al.*, Migration and differentiation of neural precursors derived from human embryonic stem cells in the rat brain. *Nat Biotechnol* **23**, 601-606 (2005).
50. M. Wernig *et al.*, Neurons derived from reprogrammed fibroblasts functionally integrate into the fetal brain and improve symptoms of rats with Parkinson's disease. *Proc Natl Acad Sci U S A* **105**, 5856-5861 (2008).
51. M. Mandai *et al.*, Autologous Induced Stem-Cell-Derived Retinal Cells for Macular Degeneration. *N Engl J Med* **376**, 1038-1046 (2017).
52. H. Q. Huo *et al.*, Modeling Down Syndrome with Patient iPSCs Reveals Cellular and Migration Deficits of GABAergic Neurons. *Stem Cell Reports* **10**, 1251-1266 (2018).
53. M. A. Israel *et al.*, Probing sporadic and familial Alzheimer's disease using induced pluripotent stem cells. *Nature* **482**, 216-220 (2012).
54. I. H. Park *et al.*, Disease-specific induced pluripotent stem cells. *Cell* **134**, 877-886 (2008).
55. A. J. Peters, S. X. Chen, T. Komiyama, Emergence of reproducible spatiotemporal activity during motor learning. *Nature* **510**, 263-267 (2014).
56. L. Regeur, B. Pakkenberg, Optimizing sampling designs for volume measurements of components of human brain using a stereological method. *J Microsc* **155**, 113-121 (1989).
57. F. W. Grillo *et al.*, Increased axonal bouton dynamics in the aging mouse cortex. *Proc Natl Acad Sci U S A* **110**, E1514-1523 (2013).
58. A. Dubbs, J. Guevara, R. Yuste, moco: Fast Motion Correction for Calcium Imaging. *Front Neuroinform* **10**, 6 (2016).

59. S. J. Barnes *et al.*, Subnetwork-Specific Homeostatic Plasticity in Mouse Visual Cortex In Vivo. *Neuron* **86**, 1290-1303 (2015).
60. R. P. Sammons, C. Clopath, S. J. Barnes, Size-Dependent Axonal Bouton Dynamics following Visual Deprivation In Vivo. *Cell reports* **22**, 576-584 (2018).